12

Acoustic Wave (TSM) Biosensors: Weighing Bacteria

Eric Olsen, Arnold Vainrub and Vitaly Vodyanoy

Abstract

This chapter is focused on the development and use of acoustic wave biosensor platforms for the detection of bacteria, specifically those based on the thickness shear mode (TSM) resonator. We demonstrated the mechanical and electrical implications of bacterial positioning at the solid-liquid interface of a TSM biosensor and presented a model of the TSM with bacteria attached operating as coupled oscillators. The experiments and model provide an understanding of the nature of the signals produced by acoustic wave devices when they are used for testing bacteria. The paradox of "negative mass" could be a real threat to the interpretation of experimental results related to the detection of bacteria. The knowledge of the true nature of "negative mass" linked to the strength of bacteria attachment will contribute significantly to our understanding of the results of "weighing bacteria." The results of this work can be used for bacterial detection and control of processes of bacterial settlement, bacterial colonization, biofilm formation, and bacterial infection in which bacterial attachment plays a role.

1. Introduction

Rapid, specific, sensitive detection and enumeration methods for microbial pathogens have long been a subject of research. This is especially true in the area of food-related illness prevention, where it's estimated that over three million deaths occur annually worldwide at a cost of $6.5–34.9 billion (Buzby and Roberts 1997) due to the consumption of food products contaminated with bacteria, bacterial toxins, or viruses (Foodborne Diseases 1997). The perceived need for instantaneous detection of pathogenic biological agents in both simple and complex matrices has increased tremendously based on the advent of sensor technologies capable of detecting macromolecules in near instantaneous or real time. To this end, specific, selective miniaturized biosensor assays that combine reliability, speed, and portability while reducing sample size and assay costs are needed to replace conventional identification techniques.

Thousands of papers have been published describing a myriad of engineering approaches for microbial biodetection since 1962, when Clark and Lyons (1962) first published their essay on a reusable enzymatic electrode. These approaches are sometimes broadly categorized into optical, calorimetric, biological-biochemical, electrochemical, and acoustic wave-mass change methods. Of these, optical methods (e.g., SPR) and acoustic wave-mass change methods appear

Eric Olsen • Clinical Investigation Facility, David Grant USAF Medical Center, Travis Air Base, CA. **Arnold Vainrub** • Department of Anatomy, Physiology, and Pharmacology, Auburn University, AL. **Vitaly Vodyanoy** • Department of Anatomy, Physiology, and Pharmacology, Auburn University, AL.

M. Zourob et al. (eds.), *Principles of Bacterial Detection: Biosensors, Recognition Receptors and Microsystems*,

to suitably combine speed, sensitivity, and portability for future development of rapid biosensors for microbial analyses (O'Sullivan and Guilbault 1999; Janshoff, Galla, and Steinem 2000; Skládal 2003).

The term "biosensor" is used rather broadly these days. As defined here, acoustic wave biosensors consist of two main components: a biological receptor that possesses affinity for an analyte of interest, and a piezoelectric transducer to convert the chemical signal of sample-receptor coupling to an amplified signal output that provides qualitative or quantitative assessment of their interaction. Acoustic waves in piezoelectric substrates (e.g., quartz) used as sensor platforms are based on mechanical waves created by an applied electric field. These waves propagate through the substrate and are then transformed back to an electric field for measurement. These discoveries have helped lead to the development of a wide range of acoustic wave devices (Morgan 2000) for applications including sensing of bacterial cells in solution.

In this chapter we will focus on the development and use of acoustic wave biosensor platforms for the detection of bacteria, specifically those based on the thickness shear mode (TSM) resonator. We also discuss the mechanical and electrical implications of bacterial positioning at the solid-liquid interface of a TSM biosensor, and present a model of the TSM with bacteria attached operating as coupled oscillators.

2. Historical Perspective, Theory and Background

2.1. Piezoelectricity and Acoustic Waves

Biosensors based on acoustic waves are rooted in numerous fundamental concepts, including the discovery of piezoelectricity by Pierre and Paul-Jacques Curie in 1880 (Curie and Curie 1880), the theory of acoustic waves as predicted by Lord Rayleigh in his 1885 analysis of surface waves in solids (Rayleigh 1885), and Augustus Love's work on acoustic waves published in 1911 (Love 1911), which included a description of shear surface waves having motion perpendicular to the sagittal plane. Subsequently, surface elastic waves were first measured in piezoelectric transducers in the 1940s and 1950s (Victorov 1967), and in 1965 White and Voltmer (1965) experimentally demonstrated direct piezoelectric coupling to surface elastic waves using an interdigital electrode transducer (IDT) on a piezoelectric plate.

Piezoelectricity refers to the generation of electrical charges in response to an applied mechanical stress. The converse is also true; application of a suitable electric field to a piezoelectric material (substrate) creates a mechanical stress, or as the name implies "converse piezoelectricity." While there are many different types of acoustic wave devices, all use the converse piezoelectric effect to produce acoustic waves. These waves propagate through a substrate, and are then transformed back to an electric field for measurement. This interconnection between piezoelectricity and acoustic waves has led to the development of a wide range of acoustic wave device applications.

2.2. Acoustic Wave Devices

The use of acoustic wave devices in electronics can be traced back more than 80 years (Morgan 2000; Gizeli 2002) and today includes timing and frequency control for applications that require extreme precision and stability such as mobile phones, satellite communications, and radio transmitters. Several of the emerging applications for these devices in the medical sciences (biological and chemical sensors) and industrial and commercial applications (vapor, humidity, temperature, and mass sensors) may eventually equal the demand of the telecommunications market.

Acoustic devices are generally described by way of their wave distribution, either through or on the surface of the piezoelectric substrate. Basically, acoustic waves differ in velocities and directions of particle movement within the substrate. Depending on the material and boundary conditions there can be different variants. Fig. 12.1 shows the configuration of typical acoustic

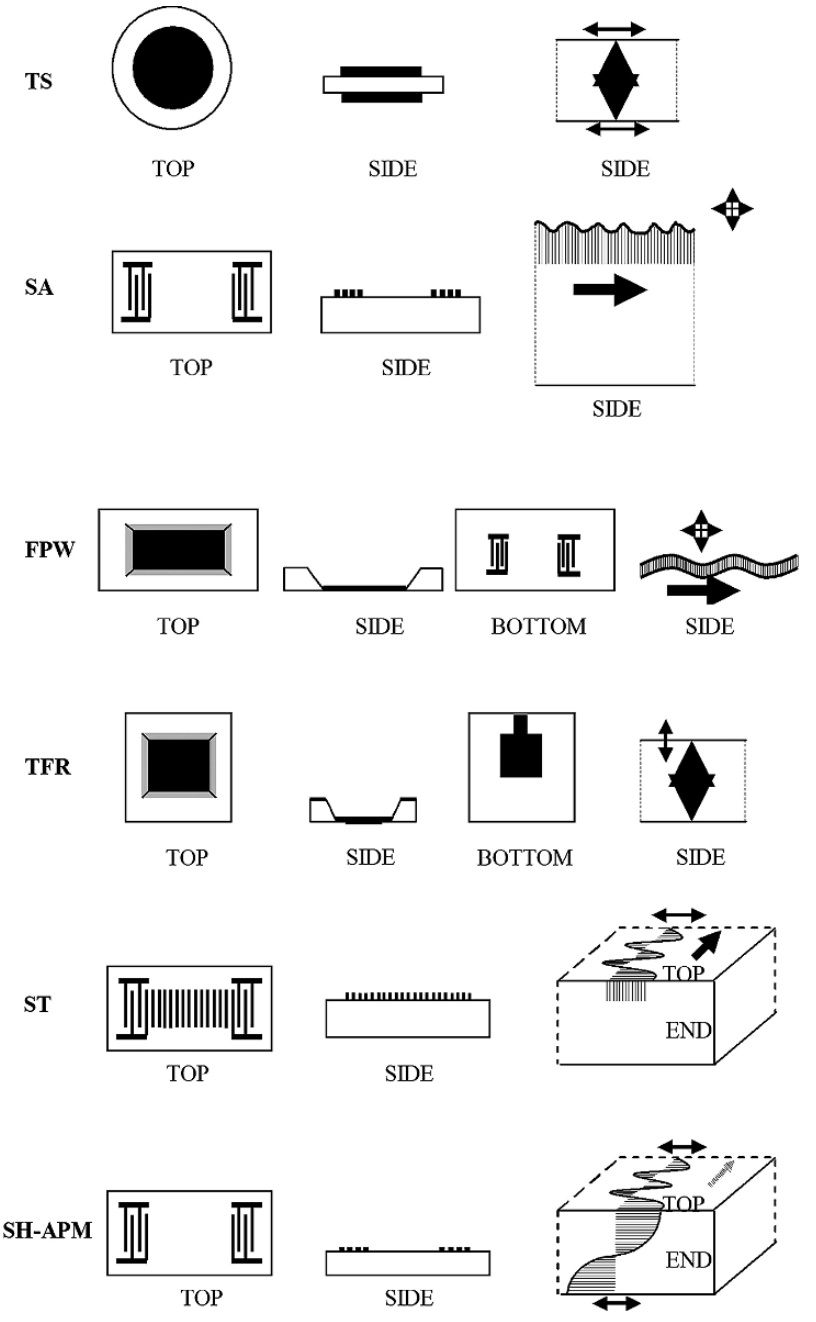

Figure 12.1. Schematic diagram showing various views of two bulk wave devices (TS and TF), two surface wave devices (SA and ST), and two plate wave devices (FPW and SH-APM). Wave motions are indicated by light arrows showing particle displacement directions and larger bold arrows showing wave propagation direction. (Grate and Frye 1996; © John Wiley & Sons Limited; reproduced with permission).

wave devices. Transverse or shear waves have particle displacements that are normal to the direction of wave propagation and which can be polarized so that the particle displacements are either parallel or normal to the sensing surface. Shear horizontal wave motion signifies transverse displacements polarized parallel to the sensing surface; shear vertical motion indicates transverse displacements normal to the surface. Some properties of selected acoustic wave devices, including TSM, transverse shear mode (i.e., QCM, quartz crystal microbalance); SAW, surface acoustic wave; STW, surface transverse wave; SH-APM, shear horizontal acoustic plate mode; FPW, flexural plate wave; and TRAW, thin rod acoustic wave, are shown in Table 12.1 (Rickert et al. 1999). A wave propagating through the substrate is called a bulk wave. The most frequently used bulk acoustic wave devices are the TSM resonator and the SH-APM. A wave propagated on the surface of a substrate is known as a surface wave. The most broadly

Table 12.1. Comparison of selected acoustic wave sensors (Rickert et al. 1999. © John Wiley & Sons Limited. Reproduced with permission)

Type	Wave type	Parameter determining the resonance frequency	Typical frequency[a] (MHz)	Typical example with: material resonance frequency (MHz) thickness d of substrate (μm) wavelength λ(μm)	Medium of preferential use
TSM (QCM)	Volume, horizontal	Thickness d	5–30	Quartz 6 270 540	Gas, liquid
SAW	Surface, vertical	Spacing of interdigital electrodes	30–500	Quartz 158 760 20	Gas
STW	Surface, horizontal	Spacing of interdigital electrodes	30–500	Quartz 250 500 20	Liquid gas[b]
Love-mode	Surface, horizontal	Spacing of interdigital electrodes and thickness d of wave guiding layer	80–300	Quartz 110 500 40	Liquid gas
SH-APM	Plate, Horizontal	Thickness d and spacing of interdigital electrodes	25–200	Quartz 101 203 50	Liquid gas[b]
FPW	Plate, vertical	Thickness d and spacing of interdigital electrodes	2–7	Zinc oxide 5.5 3.5 100	Gas liquid[c]
TRAW	Volume, longitudinal	Frequency of coupling piezoelectric transducer	0.5–8	Au[d] 1.95 50	Liquid gas[b]

[a]Material and wave velocity influence the resonance frequency in all cases.
[b]Preliminarily designed for application in liquids, but applications in gas are possible.
[c]Possible as wave velocity is less than compressional velocity of sound in liquid.
[d]The transducer itself is not piezoelectric, but acoustic waves travel through it.

used surface wave devices are the SAW and shear-horizontal surface acoustic wave (SH-SAW) sensors, also recognized as the surface transverse wave (STW) sensor. The waves are guided by reflection from multiple surfaces. Typical representatives of plate wave devices are FPW and APM.

All acoustic wave devices are sensitive to perturbations of many different physical parameters. The change in the properties of the pathway over which the acoustic wave propagates will result in a change in output signal. While all acoustic wave devices will function in gases or vacuum, only a few operate efficiently in liquids. Whether an acoustic wave device can operate in liquid is determined by the direction of the particle displacement at the surface of the device. TSM, SH-APM, and SH-SAW devices all generate waves that propagate primarily in a shear horizontal motion. A shear horizontal wave does not radiate appreciable energy into liquid, allowing functionality without excessive attenuation. Conversely, SAW devices utilizing Rayleigh waves have a substantial surface-normal displacement that radiates compression waves into the liquid and thus cannot be employed in the liquid phase (Grate and Frye 1996). An exception to this rule occurs for devices using waves that propagate at a velocity lower than that of sound in liquid. Therefore, such modes do not couple to compressional waves in liquid and are thus relatively unattenuated (Ballantine et al. 1997).

3. TSM Biosensors

Acoustic wave devices such as the TSM are essentially highly sensitive analytical balances, capable of discriminating extremely small mass deposition events. This makes them excellent analytical tools for the study of specific molecular interactions at the solid-liquid interface in air, and under vacuum or aqueous conditions (Bunde, Jarvi, and Rosentreter 1998; Cavicacute, Hayward, and Thompson 1999; Ivnitski et al. 1999; O'Sullivan and Guilbault 1999; Kaspar et al. 2000; Stadler, Mondon, and Ziegler 2003; Yakhno et al. 2007).

The TSM resonator may be better known as the quartz crystal microbalance (QCM), because its natural resonant properties are based on the piezoelectric properties of resonators prepared normally from quartz. The QCM usually consists of a thin, round AT- or BT-cut (angular orientation in relation to internal crystallography) quartz crystal wafer with two metallic electrodes (e.g., gold, silver, or palladium) deposited uniformly onto both sides of the quartz (Grate and Frye 1996). The quartz substrate can have varying dimensions and resonant frequencies, the most common being 100 kHz and 1, 2, 4, 5, 8, and 10 MHz (Scherz 2000). In itself it comprises an oscillatory circuit that can be modeled as an extended Butterworth-van Dyke equivalent circuit depending upon load conditions (Fig. 12.2) (Janshoff, Steinem, and Wegener 2004). The piezoelectric properties of the quartz result in deformation of the crystal when an electrical potential is created across the electrodes, which in turn induces a transverse, standing wave of resonance oscillation in the quartz at a fundamental frequency (Babacan et al. 2000). AT-cut crystals displace the oscillation parallel to the resonator surface and are utilized predominantly in liquids, due to their temperature stability. Any changes in the resonance frequency of the crystal are usually attributed to the effect of added mass due to binding at the active (overlapping) area of the electrodes. Theoretical modeling of the TSM response to mass accumulation has been demonstrated under various loading conditions, including ideal mass layers (thin layers of Au and SiO_2), a semi-infinite fluid (glycerol in water), and a viscoelastic layer represented by thin layers of oil (Martin, Granstaff, and Frye 1991; Bandey et al. 1999).

According to theory (Sauerbrey 1959), when a mass, m, binds at the surface of the sensor, a corresponding proportional decrease of the resonator's oscillation frequency occurs, the total quantity of which can be solved for using Sauerbrey's (1959) equation as follows, provided

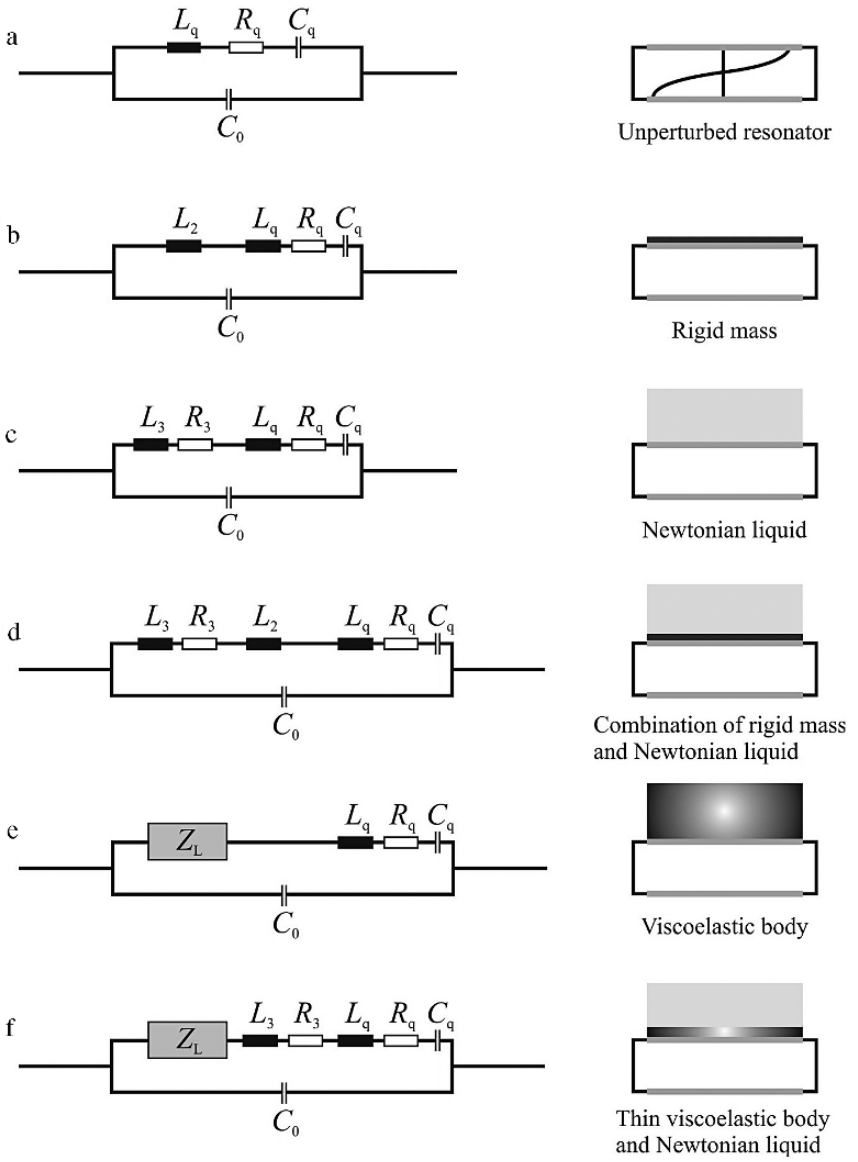

Figure 12.2. Extended equivalent circuits derived from Butterworth-van Dyke circuit for different load conditions: (a) unperturbed quartz plate; (b) rigid mass; (c) Newtonian liquid; (d) combination of rigid mass and Newtonian liquid; (e) thick viscoelastic layer; and (f) thin viscoelastic body and Newtonian liquid (adapted from Janshoff, Steinem, and Wegener 2004; with kind permission of Springer Science and Business Media).

that the mass creates a rigid, uniform film that does not slip and has the same acousto-elastic properties as quartz:

$$\Delta f = -Cf(\Delta m), \tag{12.1}$$

where Δf is the observed change in frequency (Hz) of the resonator under oscillation at its fundamental frequency due to mass loading, Cf = sensitivity factor of the resonator in Hz/ng/cm^2, and Δm = change in mass per unit area in g/cm^2.

Traditionally, the TSM has served as a mass-sensitive monitor for commercial applications such as thin-film deposition under vacuum, and electroless and electroplating processes. Sauerbrey's (1959) calculations were originally described for depositions under vacuum conditions but his theory has been extended to liquid application, as proof in concept development of sensors for biological analysis have increased dramatically in the past decade.

Acoustic wave biosensors in general have been the subject of intense research since the first analytical application reported by King (1964). As a solitary mass-sensitive transducer the device is non-specific. However, when the electrode is coated with a high affinity receptor or biorecognition component through a reliable deposition process, sample coupling between the receptor and its complementary analyte at the sensor surface can be attributed to a mass change (Rickert et al. 1999) that can be converted to a signal output, amplified, and processed to provide specific, sensitive qualitative or quantitative measurement of their interaction. Thus, a biosensor is the spatial unity of a physical transducer and a complementary biological recognition component such as an antibody, bacteriophage, DNA, or enzyme.

For more in-depth information regarding theory, the reader can consult numerous excellent references including Janshoff and Steinem (2001), and Ballantine et al. (1997).

3.1. Detection of Microorganisms

Improved characterization and modeling (Martin, Granstaff, and Frye 1991; Bandey et al. 1999) of TSM responses and functionality under liquid loading conditions have hastened development of rapid bacterial biosensors, because for the most part bacteria are naturally found under liquid conditions. There are numerous proposed applications, including use in the food industry (Leonard et al. 2003), water and environmental monitoring (Kurosawa et al. 2006), pharmaceutical sciences (Pavey 2002), bio-threat defense (Ivnitski et al. 1999; Petrenko and Vodyanoy 2003), and clinical diagnostics (Lazcka, Campo, and Munoz 2007).

The specificity of any TSM sensor is wholly dependent upon a complementary, immobilized bioreceptor. Bioreceptors for whole cell analysis generally correspond to some outside portion of the cell wall such as proteins, or possibly lipopolysaccharides or some other cell wall-associated structure (Sorokulova et al. 2005). Direct application for the detection of whole bacterial cells includes food pathogens such as *Salmonella* spp., *Escherichia coli*, and *Listeria monocytogenes;* as well as other human pathogens such as *Chlamydia trachomatis, Vibrio cholerae, Staphylococcus aureus, Pseudomonas aeruginosa*, *Mycobacterium tuberculosis, Fransicella tularensis, Legionella*, and *Bacillus anthracis* spores. A comprehensive list of selectively identified or quantitated bacterial organisms (e.g., biofilm formation in selective culturing media) using acoustic wave devices is given in Table 12.2. Also, acoustic wave biosensors have been used for the direct detection of other microorganisms including human, plant, and bacterial viruses such as coronavirus (Zuo et al. 2004), tobacco mosaic virus (Dickert et al. 2004), dengue virus (Su et al. 2003), hepatitis A and B (Konig and Gratzel 1995), rotavirus and adenovirus (Konig and Gratzel 1993), cymbidium mosaic potexvirus and odontoglossum ringspot tobamovirus (Eun et al. 2002), and M-13 phage (Uttenthaler et al. 2001); yeast (Muramatsu et al. 1986; Hayden and Dickert 2001; Hayden, Bindeus, and Dickert 2003); and even algae (Nakanishi et al. 1996).

Acoustic wave biosensors have also been used for indirect detection of microorganisms through the detection of corresponding: DNA from *E. coli* O157:H7 (Deisingh and Thompson 2001; Mo et al. 2002; Mao et al. 2006), hepatitis A virus (Zhou et al. 2002), and human papilloma virus (Wang et al. 2002); specific bacterial protein products for *E. coli* (Nanduri et al. 2007); antigenic proteins from dengue virus (Wu et al. 2005; Tai et al. 2006);

Table 12.2. Acoustic wave (AWD) biosensors developed for bacterial detection

Bacterium	AWD	Receptor	LLOD	Reference
Bacillus subtilis	PM	NS	–	(Ishimori, Karube, and Suzuki 1981)
Bacillus thringiensis spores	SHSAW	Ab	1764 spores	(Branch and Brozik 2004)
Chlamydia trachomatis	TSM	Ab	260 ng/mL	(Ben-Dov, Willner, and Zisman 1997)
Escherichia coli	TSM	NS	–	(Zhang et al. 2002)
Escherichia coli	TSM	NS	10 cells/ml	(He et al. 1994)
Escherichia coli	TSM	NS	–	(Otto, Elwing, and Hermansson 1999)
Escherichia coli	TSM	NS	–	(Zhao, Zhu and He 2005)
Escherichia coli	TSM	SIP	unknown	(Dickert et al. 2003)
Escherichia coli	SSBW	Ab	400 cells/ml	(Deobagkar et al. 2005)
Escherichia coli	TSM	NS	–	(He and Zhou 2007)
Escherichia coli	SHSAW	Ab	10^6 cells/ml	(Moll et al. 2007)
Escherichia coli	SHSAW	Ab	$\sim 10^9$ cells/ml	(Berkenpas, Millard and Pereira da Cunha 2006)
Escherichia coli	SHSAW	Ab	$10^5 - 10^6$ cells/ml	(Howe and Harding 2000)
Escherichia coli	TSM	Ab	10^3 cells/ml	(Su and Li 2004)
Escherichia coli	TSM	Ab	1.7×10^5 cells/ml	(Kim, Rand, and Letcher 2003)
Escherichia coli	FPW	Ab	3.0×10^5 cells/ml	(Pyun et al. 1998)
Fransicella tularensis (Ft)	TSM	Ft antigen	5×10^6 cells/ml	(Pohanka and Skládal 2005)
Klebsiella sp.	PM	NS	–	(Ishimori, Karube, and Suzuki 1981)
Legionella	SHSAW	Ab	10^6 cells/ml	(Howe and Harding 2000)
Listeria monocytogenes	TSM	Ab	1.0×10^7 cells/ml	(Vaughan, O'Sullivan, and Guilbault 2001)
Milk bacteria*	TSM	NS	–	(Chang et al. 2006)
Mixed bacteria**	TSM	NS	–	(He et al. 2006)
Mycobacterium tuberculosis	TSM	Ab	10^5 cells/ml	(He and Zhang 2002)
Mycobacterium tuberculosis	TSM	NS	2×10^3 cells/ml	(He et al. 2003)
Proteus sp.	TSM	NS	–	(Yao et al. 1998)
Proteus vulgaris	TSM	NS	120 cells/ml	(Tan et al. 1997)
Proteus vulgaris	TSM	NS	340 cells/ml	(Deng et al. 1997)
Proteus vulgaris	TSM	NS	–	(Bao et al. 1996b)
Pseudomonas aeruginosa	TSM	NS	3.3×10^5 cells cm^{-2}	(Niven et al. 1993)
Pseudomonas aeruginosa	TSM	NS	60-100 cells/ml	(Zhao, Zhu and He 2005)
Pseudomonas aeruginosa	TSM	Ab	1.3×10^7 cells/ml	(Kim, Park, and Kim 2004)
Pseudomonas aeruginosa	TSM	NS	–	(Reipa, Almeida, and Cole 2006)
Salmonella sp.	TSM	Ab	3.2×10^6 cells/ml	(Park, Kim and Kim 2000)
Salmonella serotypes A,B,D	TSM	Ab	10^5 cells/ml	(Wong et al. 2002)
Salmonella typhimurium	TSM	Ab	10^3 cells/ml	(Bailey et al. 2002)
Salmonella typhimurium	TSM	Ab	100 cells/ml	(Olsen et al. 2003)
Salmonella typhimurium	TSM	Phage	0 cells/ml	(Olsen et al. 2006)
Salmonella typhimurium	TSM	Ab	100 cells/ml	(Pathirana et al. 2000)
Salmonella typhimurium	TSM	Phage	100 cells/ml	(Olsen et al. 2007)
Salmonella typhimurium	TSM	Ab	1.5×10^9 cells/ml	(Babacan et al. 2000)
Salmonella typhimurium	TSM	Ab	10^7 cells/ml	(Babacan et al. 2000)
Salmonella typhimurium	TSM	Ab	5.3×10^5 cells/ml	(Ye, Letcher, and Rand 1997)
Salmonella typhimurium	TSM	Ab	10^5 cells/ml	(Prusak-Sochaczewski and Luong 1990)
Salmonella typhimurium	TSM	Ab	$10^5 - 10^6$ cells/ml	(Su and Li 2005)
Salmonella typhimurium	TSM	Ab	100 cells/ml	(Kim, Rand, and Letcher 2003)
Salmonella typhimurium	TSM	Ab	9.9×10^5 cells/ml	(Park and Kim 1998)
Salmonella paratyphi A	TSM	Ab	170 cells/ml	(Fung and Wong 2001)
Salmonella paratyphi A	TSM	Ab	10^5 cells/ml	(Si et al. 1997)
Salmonella enteriditis	TSM	Ab	1.0×10^5 cells/ml	(Si et al. 2001)
Salmonella enteriditis	TSM	Ab	1.0×10^5 cells/ml	(Ying-Sing, Shi-Hui, and De-Rong 2000)

Table 12.2. (Continued)

Bacterium	AWD	Receptor	LLOD	Reference
Staphylococcus aureus	TSM	Ab	5×10^5 cells/ml	(Le et al. 1995)
Staphylococcus epidermidis	TSM	Fibronectin	100 cells/ml	(Pavey et al. 2001)
Staphylococcus epidermidis	TSM	NS	100 cells/ml	(Bao et al. 1996a)
Streptococcus mutans	TSM	NS	–	(Kreth et al. 2004)
Vibrio cholerae	TSM	Ab	4×10^4 cells/ml	(Carter et al. 1995)

Ab = corresponding antibody; NS = not selective (e.g. for biofilm monitoring) or some other means of selectivity (e.g. specific culture media) was used other than attached bioreceptor; PM = piezoelectric membranes; SIP = surface imprinted polymer layer; SSBW = surface skimming bulk wave; * = non-specific detection of bacterial growth in milk; ** = non-specific detection of bacterial growth in blood culture bottles.

antibodies from bacteria including *Helicobacter pylori* (Su and Li 2001), *Treponema palladium* (Aizawa et al. 2001), *Salmonella enteritidis* (Su et al. 2001), *Francisella tularensis* (Pohanka and Skládal 2005), and *Staphylococcus epidermidis* (Pavey et al. 1999), the helminth *Schistosoma japonicum* (Wu et al. 1999, 2006), and African swine fever virus (Uttenthaler, Kolinger, and Drost 1998); and bacterial toxins from *E. coli* including LT (Spangler et al. 2001), Stx (Uzawa et al. 2002), and an unidentified endotoxin (Qu et al. 1998), and *Staphylococcus* including SEB and C2 toxins (Harteveld, Nieuwenhuizen, and Wils 1997; Gao, Tao, and Li 1998; Lin and Tsai 2003). Additionally, new innovations such as gas chromatography coupled to SAW technology have been used for indirect detection of *Klebsiella pneumoniae, Pseudomonas aeruginosa, Escherichia coli,* and two *Candida albicans* yeast strains (Casalinuovo et al. 2005). Ion chromatography combined with TSM has been used to monitor *Lactobacillus* fermentation through lactic acid production (Zhang et al. 2001).

As shown in Table 12.2, the overwhelming majority of acoustic wave biosensors described in the literature for direct detection of whole bacterial cells is based on the TSM platform, with the most frequently targeted organism being *Salmonella,* specifically *S. typhimurium. Salmonella* is a leading etiology of foodborne illness and death in the U.S. (Mead et al. 1999).

Prominent acoustic wave sensors for *Salmonella* include those of Prusak-Sochaczewski and Luong (1990), who reported the first QCM assay for *Salmonella* with an assay time of 50–60 s, a lower detection limit of 10^5 cells/ml, and 0.5–5 hour incubation period, depending on the concentration of the microbial suspension; Park and Kim (1998), whose thiolated immunosensor possessed an assay time of 30–90 minutes, a lower detection limit of 9.9×10^5 cells/ml, and a detection range up to 1.8×10^8 cells/ml; Ye, Letcher, and Rand (1997), whose linear (R = 0.942) biosensor assay for *S. typhimurium* had a 25 min response time, a lower detection limit of 5.3×10^5 CFU/ml, and a range up to 1.2×10^9 CFU/ml; Pathirana et al. (2000), who developed an antibody-based TSM sensor to detect *Salmonella typhimurium* in poultry that possessed rapid analytical response times of 79 ± 20 seconds, linear ($R > 0.98$, $p < 0.01$) dose-response over 5 decades (10^2 to 10^7 cells/ml) of bacterial concentration, sensitivity of 18 ± 5 mV/decade of *S. typhimurium* concentration, and a detection range of 350 ± 150 to 10^{10} cells/ml; and the sensors of Babacan et al. (2000, 2002), Park, Kim and Kim (2000), Su and Li (2005), and Kim, Rand, and Letcher (2003).

3.2. Measurement in Liquid

TSM functionality in liquids is complex. Influences from numerous non-gravimetric contributions include liquid viscosity and density (Bandey et al. 1999); surface free energy (Thompson et al. 1991); roughness, surface charge density, and water content of biomolecules

(Janshoff and Steinem 2001); pressure and temperature (Niven et al. 1993); and the viscoelasticity and interfacial effects (Lucklum 2005) of thin films deposited in the form of bioreceptors. Therefore, the use of Sauerbrey's (1959) equation to strictly quantitate mass deposited to the solid-liquid interface under liquid conditions is controversial. Sauerbrey's equation was developed based on the oscillation of TSM in vacuum and only applies to thin, uniform, rigid masses attached tightly to the crystal. Thus, frequency response under liquid conditions cannot solely be attributed to mass deposition (Gizeli 2002; Lucklum 2005). For example, TSM sensors exposed to relatively large protein and polysaccharide molecules in solution have also been shown to give responses that did not correlate with mass changes at the solid-liquid interface (Ghafouri and Thompson 1999). The authors ascribed this phenomenon to viscoelastic and acoustic coupling at the interface. One could expect especially complicated interfacial properties when the TSM sensor is exposed to larger biological entities such as bacterial cells. Electromechanical forces created by live and moving organisms may contribute to the apparent mass of binding bacteria. Additionally, factors such as nutrition, growth, differentiation, chemical signaling, and mutagenic exposure may also factor in controlling the physiological state of binding bacteria. A bacterial cell (e.g., *E. coli*) can possess a mass of approximately 665 fg, making it one million times heavier than a typical (150 kD) antibody molecule (Neidhardt 1987) used as a bioreceptor. Bacteria carry out or are involved with various movements including flagellation, Brownian motion, chemotaxis, swimming behavior, adaptation, and other cell phenomena (Alberts et al. 1994). Bacterial binding on sensor surfaces may also depend on the presence of fimbriae (Otto, Elwing, and Hermansson 1999), flagella (Sorokulova et al. 2005), or other surface-associated adhesion factors, as well as the ability of single cells to associate and form colonies. Bacterial interaction with a biosensor may also be highly dependant upon environmental conditions (Olsen et al. 2003).

Notwithstanding, the ability to function in liquid environments conducive to bacterial growth and the fact that mass can be sensitively and specifically differentiated as a molecular recognition/binding event at the solid-liquid interface are two good reasons the TSM is being developed as a rapid detection tool. Normally, the TSM sensor is enclosed within a cell into which fluids are injected ("flow injection analysis") or flowed via a peristaltic pump. Numerous examples are available by reviewing the references in Table 12.2. While "closed systems" are prevalent and rather simple in operation, solutions can also be simply applied by pipette directly to the surface of the TSM, or what can be contrasted as an "open system," where fluids are directly applied to the sensor surface (Olsen et al. 2003, 2006). Systems have also been devised for air-borne sample-to-liquid transfer (Frisk et al. 2006) to facilitate acquisition of airborne threat agents such as *Bacillus anthracis* spores.

3.3. TSM Biosensor Characteristics

Bacterial binding as the signal output of the transducer has been measured and analyzed using many different formats to give a detailed analysis of surface/interface changes, including fundamental resonance and/or overtone frequency shift, frequency shift with dissipation, voltage, resistance and capacitance, and acoustic impedance. Absolute or differential (Δf) frequency changes alone due to binding are given by most authors and appear to be acceptable and sensitive as a measurement of sensor functionality. For example, Fig. 12.3a shows typical frequency response curves of a prepared (phage) biosensor tested with logarithmic concentrations of *S. typhimurium* ranging from 0 (PBS)–10^7 cells/ml. For each concentration, the sensor quickly comes to steady-state equilibrium within several hundred seconds following specific phage-bacteria binding at the solid-liquid interface. Plotting the mean values of steady-state frequency readings as a function of bacterial concentration (Fig. 12.3b) gives a high dose-response relationship ($R = -0.98$, $p < 0.001$), small signal to noise ratio (–10.9 Hz) measured as the slope

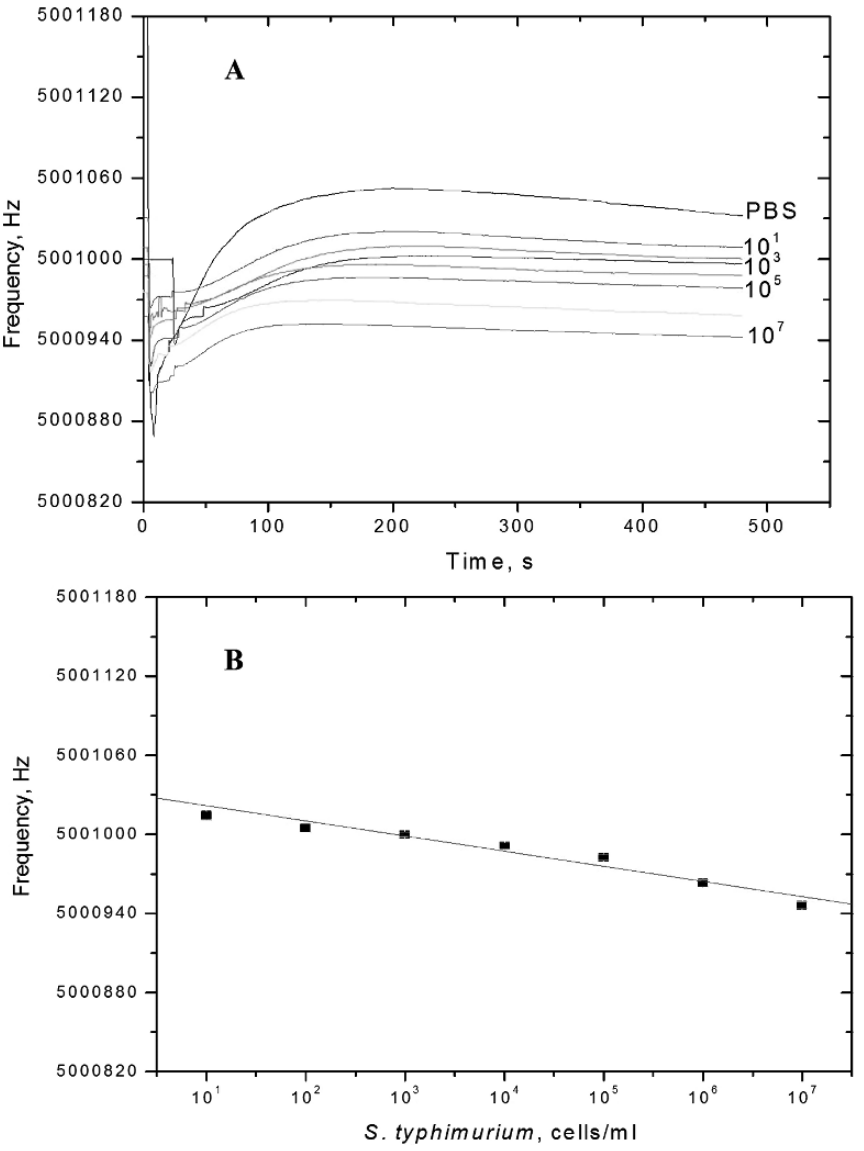

Figure 12.3. (A) Frequency responses of phage biosensor to increasing concentrations of *S. typhimurium* as a function of time. (B) Dose-response relation of mean values ($n = 2800 \pm 2$) of steady-state output sensor frequencies as a function of *S. typhimurium* concentration. Bars are SD = 2.9 – 10.0 Hz. Curve is linear least squares fit to experimental data ($R = -0.98$, slope = −10.9 Hz, $p < 0.001$) (reprinted from Olsen et al. (2006), with permission of Elsevier).

of the linear portion of the dose-response, linearity over six decades of bacterial concentration, and a lower limit of detection at 100 cells/ml, well below the infectious dosage of *Salmonella.*

Other authors (Otto, Elwing, and Hermansson 1999) attempt to determine dissipation in the system (ΔD) as a quantitative measure of system damping, usually due to lossy or viscoelastic films or near surface interaction of the bacteria. Resistance (R), capacitance (C), and/or impendence (L) measurements are sometimes determined (He et al. 2003; Kim, Rand, and Letcher 2003; Su and Li 2005) through a high frequency impedance analyzer based on the TSM as an RLC series equivalent circuit.

There are many other characteristics of TSM platforms that require consideration when developing and testing biosensors, including:

- **Specificity:** the strength of the interaction between a molecular probe (e.g., antibody) and an antigen (target analyte) as estimated by the dissociation constant K_d. The smaller the K_d the higher the specificity of binding. The free energy of dissociation (ΔG_d) of a ligand-receptor complex is related to its equilibrium dissociation constant K_d by the equation:

$$\Delta G_d = -kT \ln(K_d/K_0), \tag{12.2}$$

  where k is a Boltzmann constant and T is a temperature in °K. The equation refers to a standard reference state where all chemical species are 1 M (i.e., $K_0 \sim 0.6\,\text{molecules/nm}^3$) and attributes a free energy of zero to a complex with a dissociation constant of 1 M (Chothia and Janin 1975).
- **Binding selectivity:** is defined by a selectivity coefficient (K). Binding selectivity can be estimated from dose responses of a biosensor to different analytes (e.g., bacteria). The signal response V as a function of the primary analyte (e.g., bacteria) concentration (C) can be represented by the following empirical equation:

$$V = A + S \log C, \tag{12.3}$$

  where C is the primary analyte concentration, A is the constant, and S is the slope of the dose response dependence, defined as the sensitivity of the sensor (Pathirana et al. 1996).

  The selectivity coefficient for any other analyte to the primary analyte (e.g., bacteria) (K) can be determined from the signal responses at different concentrations using a method similar to the matched potential method (Pathirana et al. 1996; Umezawa 1996). The selectivity coefficient is defined as the concentration ratio (R) of primary to interfering species $[\Delta(C_p)/\Delta(C_i)]$, which gives the same response change at the same condition. Using the definition of the selectivity coefficient and Eq. 12.2, the following is derived:

$$R = C_p/C_i, \tag{12.4}$$

$$K = R = S_i/S_p, \text{ when } \Delta C_p \text{ approaches zero}, \tag{12.5}$$

  where S_p and S_i are slopes of signal responses to primary and interfering species (other bacteria), respectively.
- **Sensitivity:** The change of the biosensor's output signal when the analyte content (total quantity or concentration) changes by one unit. For non-linear sensors, the sensitivity depends on the analyte level and is given by the slope of the sensor's output curve versus the analyte content.
- **Detection threshold.** The ability of the biosensor to discriminate an analyte (e.g., bacteria) from background at the lowest quantity of analyte in the testing solution.
- **Dynamic or Working Range:** The range of the analyte content over which the sensor can perform qualitative or quantitative detection.
- **Linear range:** That part of the dynamic range where the sensor's output is a linear function of the analyte content.

- **Saturation:** The level at which the sensor no longer functions correctly. For biosensors, this is usually the point where the bioreceptor has been saturated with analyte and reaches a peak signal.
- **Response Time:** The amount of time required to detect the analyte as given by the signal output.
- **Accuracy:** Closeness of the sensor measurement result to the actual quantity of cells in solution. Actual quantity of cells (usually stated in reports as cells/ml) is found from traditional plate culture of the organism. Optical counting methods are also possible (Olsen 2000).
- **Stability:** The ability of the sensor signal to give a constant, steady output signal when measuring a steady input, such as a load of cells.

3.4. Commercial TSM Microbalances

Traditionally, the TSM has served as a mass-sensitive monitor in commercial applications such as thickness monitoring and deposition rate control for thin films under vacuum, and for electroless and electroplating processes (Krause 1993). The functionality of the TSM under liquid conditions has increasingly driven adaptation to the development of extremely sensitive biosensors in the past decade. Total QCM systems are relatively inexpensive and simple in operation, requiring for the most part only the resonator crystal, external oscillatory circuit, and frequency counter. Many of the systems described in the literature for sensor developments are pieced together or custom built and may additionally include impedance analyzers, thermostatic jacketing for temperature control, and pump or flow injection equipment. With the advent of the Internet, numerous commercial QCM products including crystal resonators and holders, frequency monitors, flow cells, and even entire systems are now easily available throughout the world, making entry into this field reasonable in terms of cost and availability. A recent review of the Internet yielded numerous larger manufacturers and suppliers of complete QCM systems (Table 12.3).

One such commercially available microbalance produced by Maxtek Inc. can be used for both biosensor preparation and testing and consists of a 50 cm sensor probe connected by a tri-axial cable to a precalibrated plating monitor (Fig. 12.4). This system is often used in electroplating processes within vats, necessitating the long probe and open face exposed to solution. The plating monitor has a frequency resolution of 0.03 Hz and mass resolution of $0.375\,ng/cm^2$ at 5 MHz. TSM transducers are precleaned AT-cut plano-plano quartz liquid-plating resonators possessing a 5 MHz nominal resonant frequency. Resonators (2.54 cm diameter, 333 μm thickness) have gold plated electrodes evaporated onto titanium adhesion layers on both the top and bottom (Fig. 12.5). The electrodes are polished to an average surface roughness of approximately 50 Å. This minimizes liquid entrapment within the pores at the crystal surface, reducing the creation of apparent mass loadings under liquid measurement conditions. Also, resonators are pretested to assure conformance to critical accuracy specifications required for reproducibility, and rate and thickness measurements (PM-740 series operation and service manual 1996). Both the bioreceptor, during sensor preparation (Fig. 12.6a), and the analyte, during sensor testing, can be directly applied to the surface of the sensor by pipette (Fig. 12.7). Absolute frequency readings from the sensor are transferred to a PC directly from the plating monitor or via a multimeter, in which case voltage readings can be captured (Pathirana et al. 2000). The sensor probe, attached to the stand, and all necessary components of the experiment can be contained at room temperature within an Atmosbag™ gloved isolation chamber (Sigma-Aldrich, Milwaukee, WI) inflated with inert nitrogen gas during bioreceptor deposition studies to prevent possible contamination of the resonator by particulate matter.

Table 12.3. Selected commercially available QCM systems

Company	Internet URL (http://)	QCM products
Maxtek, Inc.	www.maxtekinc.com	RQCM, crystals and holders oscillators, flow/liquid cells, thin-film monitors/controllers
Q-Sense	www.q-sense.com	E4 QCM-D, D300; EQCM, crystals
Universal Sensors, Inc.	intel.ucc.ie/sensors/universal	PZ-105, crystals, flow cells
Seiko EG&G	speed.sii.co.jp/pub/segg/hp	QCM934, QCA922
Princeton Applied Research	www.princetonappliedresearch.com	QCM922, EQCM
ICM, Inc.	www.qcmsystems.com/index.html	crystals, oscillators, flow cells
QCM Research	www.qcmresearch.com	CQCM, TQCM, Mark 21 QCM Thin-film controllers
Tectra	www.tectra.de/qmb.htm	MTM-10 thin film monitors/controllers
KSV Instruments, LTD	www.ksvltd.com	QCM-Z500, crystals, EQCM flow cells, pumps, temp control unit, spin-coater/holder
SRS	www.thinksrs.com	QCM-100, QCM-200, EQCM, crystals and holders, oscillators thin-film controllers, flow cells
Masscal	www.masscal.com	G1 QCM
Faraday Labs	www.faradaylabs.com	QCM
Initium, Inc.	www.initium2000.com	Affinix Q
Sigma Instruments	www.sig-inst.com	Q-pod, SQM-160, crystals, thickness/rate monitors
Tangidyne	www.tangidyne.com	Optical crystals and holders
Technochip	www.technobiochip.com	μLibra QCM, EQCM, "Electronic Nose"

In addition to some of the previously mentioned TSM characteristics, some additional factors to consider before purchasing commercially available equipment include cost, resolution, reproducibility, reliability, ruggedness, analytical range, speed, noise, cost, power requirements, space limitations, availability, technical servicing/maintenance, life expectancy, data capture capabilities, ease of use, and other analytical capabilities and adaptabilities such as use under differing temperatures, pressures, or other environmental conditions, and adaptability to peripheral devices such as voltmeters, PC, peristaltic pumps, and thermostatic jacketing.

Like all other sensory devices, the TSM as a sensor platform has its advantages and drawbacks. In addition to addressing necessary characteristics of TSM biosensors such as speed, accuracy, precision, sensitivity, and specificity, several other factors should be considered, including incubation time of analyte, numerous steps including application of analyte and washing and drying, regeneration of the sensor surface if reusability is a factor, and total cost of assay to include resonators, reagents, bioreceptors, etc.

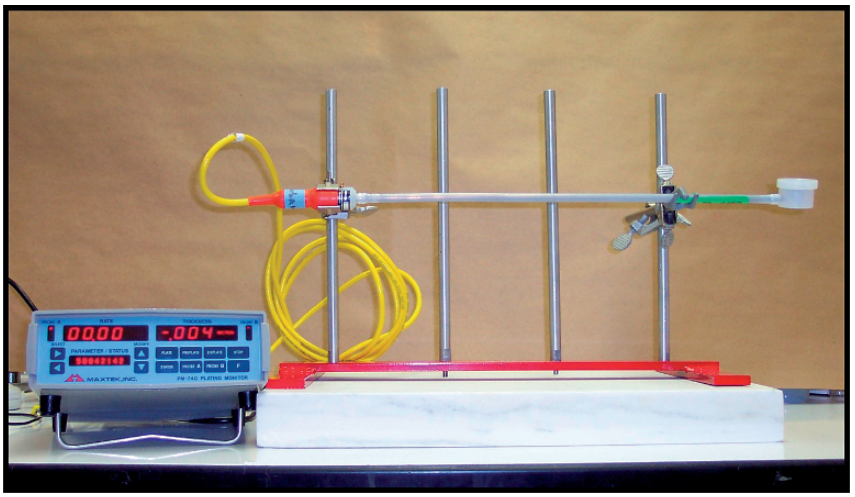

Figure 12.4. QCM platform for deposition and biosensor measurements. A plating monitor was connected to a sensor probe that was horizontally clamped to a lattice stand then tilted 10° transverse to the stand. The sensor probe and stand were positioned atop a marble slab to reduce extraneous environmental vibrations.

3.5. Immobilization of Probes onto Sensor Surface

A major drawback to the TSM as a sensor is its non-specificity. Anything that can and will attach to it under liquid loading conditions can be recognized as a molecular binding event. Therefore, application of bioreceptors is necessary in order to affect specificity towards the analyte of choice (bacteria, bacteria components, toxins, or complementary DNA, etc.). The sensing properties of a sensor depend on the physical-chemical environment of antibody and antigen-antibody complex, which are in turn determined by antibody immobilization techniques (Ahluwalia et al. 1992; Storri, Santoni, and Mascini 1998). While the TSM can be very quick in its measurement, building the sensor with bioreceptors can be a tedious, multi-step process that can take numerous hours or even days. Additionally, and possibly the greatest consideration,

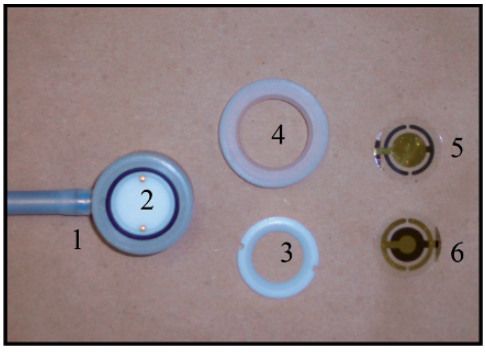

Figure 12.5. Maxtek sensor probe and associated components: (1) housing for external oscillatory circuit electrical contacts; (2) crystal holder cavity with o-ring (black) installed. The gold index pins that contact the reverse electrode of the resonator are clearly visible; (3) teflon resonator retainer ring; (4) threaded retainer ring cover; (5) sensing electrode of polished, 5 MHz AT-cut thickness shear mode quartz resonator; (6) contact electrode of quartz resonator. The "active area" of the resonator is that central portion of the sensing electrode that overlaps the contact electrode ($\approx 34.19\,mm^2$).

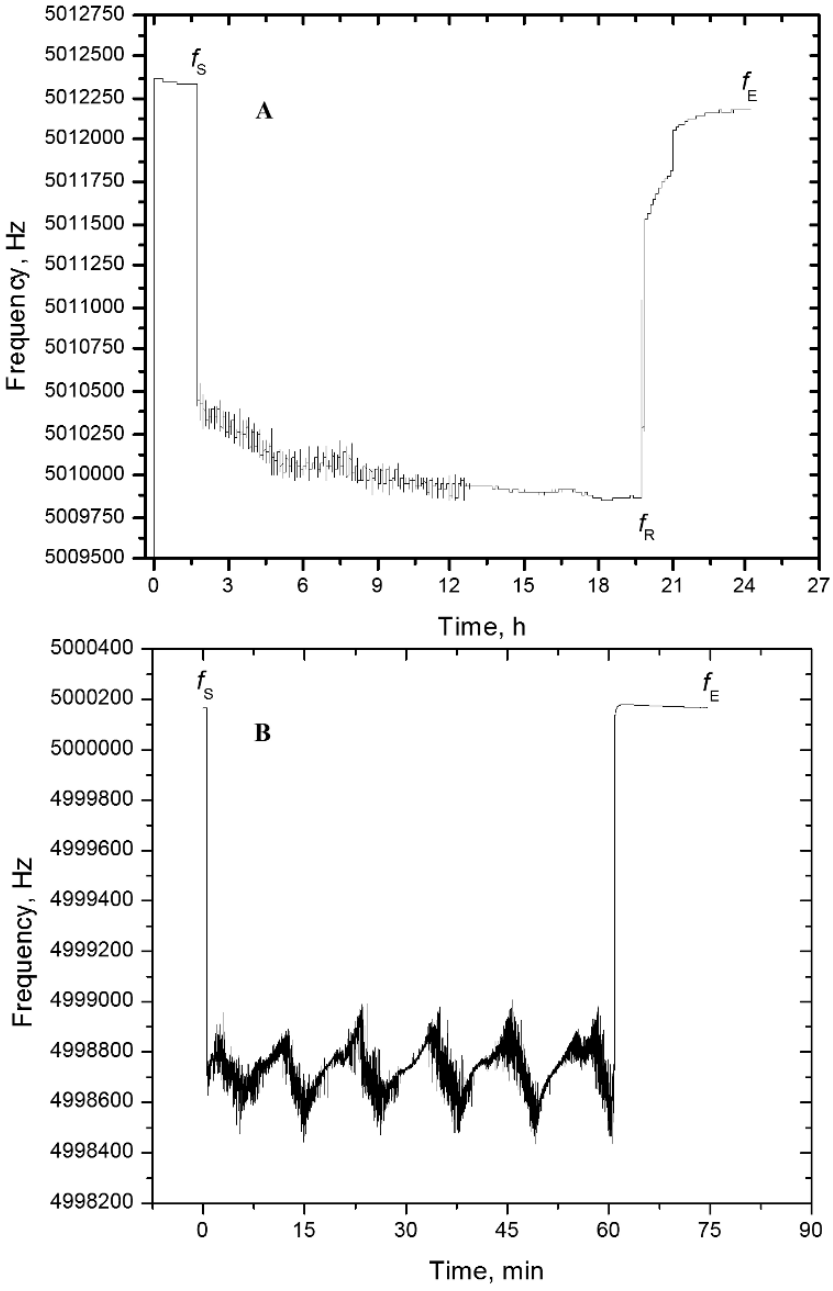

Figure 12.6. (A) Representative line graph depicting frequency change as a function of phage binding to the resonator over time. Eighteen-hour incubation period is shown. f_S: Application of phage solution to clean, dry resonator at steady state: 5,012,338 Hz. f_R: Removal of phage solution, washing, and drying of resonator. f_E: Dried resonator at steady state: 5,012,177 Hz. $\Delta f = (f_S) - (f_E) = -161$ Hz. (B) Representative line graph of a clean resonator with degassed water only (control) depicting frequency change as a function of time. One-hour incubation period is shown. f_S: Application of water to clean, dry resonator at steady state: 5,000,167 Hz. f_E: Dried resonator at steady state: 5,000,167 Hz. $\Delta f(f_S) - (f_E) = 0$ Hz (reprinted from Olsen et al. (2006), with permission of Elsevier).

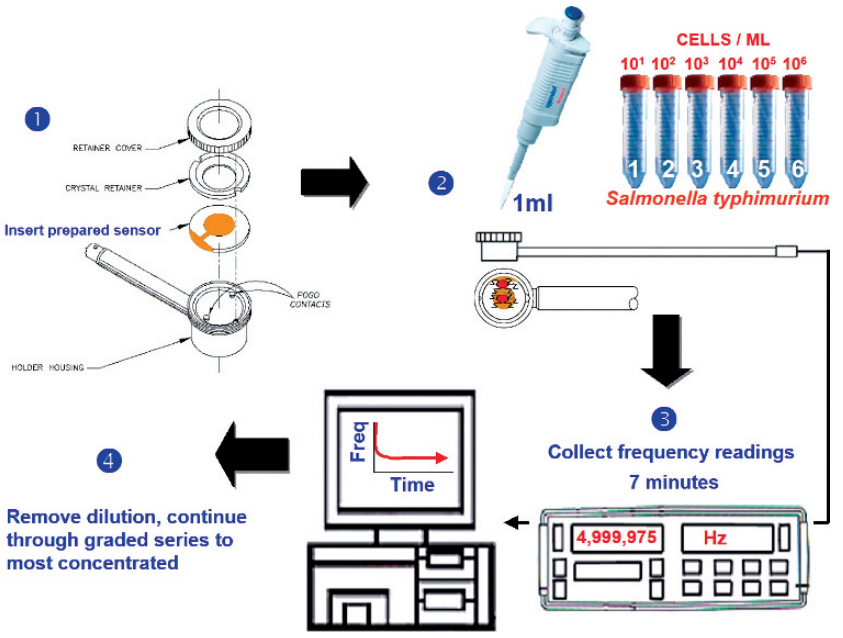

Figure 12.7. Testing scheme for biosensors: (1) Prepared biosensor was installed into sensor probe; then (2, 4) tested with a graded series of *S. typhimurium* test solutions; and (3) frequency (or voltage) output of sensor was recorded for data analysis.

is the reproducibility of the bioreceptor immobilization process. An in-depth analysis of the techniques of probe immobilization onto sensor surfaces is presented in the following sections.

3.5.1. Physical Adsorption

The most common techniques involve direct bonding of an antibody receptor to a reactive group coupled to the surface. The coupling agent and reactive group are generally selected to match the chemistry of the specific antibody. However, the adsorption process is difficult to control and the amount of protein adsorbed to most solid surfaces is usually below that which would correspond to a close-packed monolayer. Further, during the adsorption, the exposure of internal hydrophilic groups of proteins to hydrophobic surfaces causes a decrease in the activity and specificity of the protein/target interactions. In spite of these shortcomings of this method, direct physical adsorption is the simplest way of antibody immobilization on the sensor surface. This method has been successfully employed for immobilization of a wide range of biological elements directly onto piezoelectric electrodes, including anti-human serum albumin (Muratsugu et al. 1993), IgG (Minunni, Skladal, and Mascini 1994), goat anti-ricin antibody (Carter et al. 1995a), anti-*Vibrio Cholera* (Carter et al. 1995a), African swine fever virus protein (Uttenthaler, Kolinger, and Drost 1998), recombinant protein fragments of HIV specific antibodies (Aberl and Wolf 1993), filamentous phage (Sykora 2003; Olsen et al. 2006; Nanduri et al. 2007; Olsen et al. 2007), lytic phage (Balasubramanian et al. 2007), and designer peptides (Selz et al. 2006). Protein molecules adsorb strongly and irreversibly on gold surfaces due to hydrophobic actions (Horisberger 1984, 1992).

Quantitative "dip and dry" deposition experiments can be used to monitor physical adsorption of bioreceptors in the preparation of biosensors (Olsen et al. 2006). Dip and dry, as described by Prusak-Sochaczewski and Luong (1990), is the change in the resonant frequency,

Table 12.4. Quantity of filamentous phage physically adsorbed to resonators as a function of time

Incubation (min)	$-\Delta f$ (Hz)	Δm (ng)[d]	Phage adsorbed (virions)[e]
20	45[a]	795	1.80×10^{10}
40	60[b]	1065	2.41×10^{10}
60	92[c]	1625	3.68×10^{10}
1080	136	2402	5.45×10^{10}
1440	163	2880	6.50×10^{10}

[a]Mean average of 5 experiments, SD = 31.1 Hz.
[b]Mean average of 3 experiments, SD = 46.5 Hz.
[c]Mean average of 4 experiments, SD = 59.2 Hz.
[d]Adsorbed phage mass as determined by Sauerbrey equation, $\Delta f = (0.0566)(\Delta m)$.
[e]Quantity of phage deposited to the active area (34.19 mm^2) of the upper sensing electrode as calculated from $\Delta m/m_\nu$, where the mass of a single virion (m_ν) is 2.66×10^7 dal / 6.023×10^{23} dal = 44.1×10^{-9} ng.

Δf, of a dry TSM resonator prior to and after mass deposition. Using Sauerbrey's (1959) equation, the physical adsorption of phage as a function of time can be determined. For example, Fig. 12.6a shows steady-state oscillation of a dry, clean resonator prior to the application of 1 ml of diluted stock phage E2 in suspension (6.7×10^{10} virions/ml) (f_S), followed by an 18 h incubation period at room temperature, removal (f_R) of the phage suspension and washing with degassed water, and finally drying, with a subsequent return to steady-state resonance (f_E). The resulting frequency change, Δf, measured as a decrease, $f_S - f_E$, was –161 Hz, indicating that phage adsorbed to the resonator. This can be contrasted to a control (Fig. 12.6b) consisting of a clean TSM resonator tested with degassed water only, which indicated no frequency change ($f_S - f_E = 0$ Hz). Resonance frequency changes due to phage adsorption were determined for periods up to 24 h (1440 min) (Table 12.4). When the quantity of adsorbed phage is graphed as a function of time the majority of phage appeared to adsorb within the first few hours after deposition was started (Olsen et al. 2006). The quantity of phage in virions can be calculated from the total adsorbed biomass, Δm, by estimating the mass of a single recombinant fd-tet phage at 2.66×10^7 daltons, based on 4000 pVIII outer coat proteins, each containing 55 amino acids with a total molecular weight of 2.35×10^7 (Kouzmitcheva 2005), and DNA with a molecular weight of 3.04×10^6 (Petrenko 2007). As shown in Table 12.4, the total number of phage particles deposited to the TSM resonator ranged from $1.8 \times 10^{10} - 6.5 \times 10^{10}$ virions as a function of exposure time (20 min –24 h, respectively) to phage in solution. Phage deposition to the TSM was confirmed in real time by fluorescence microscopy for a period of two consecutive hours and characterized by strong, non-reversible binding under aqueous conditions (Olsen et al. 2006).

3.5.2. Other Coupling Methods

To overcome disadvantages of a direct physical adsorption method, a range of immobilization methods have been suggested, including lipid bilayer entrapment (Ramsden 1997a, 1997b, 1998, 1999, 2001), thiol/disulfide exchange, aldehyde and biotin-avidin coupling (Mittler-Neher et al. 1995), photo-immobilization to photolinker-polymer-precoated surfaces (Gao et al. 1994), molecular imprinted polymer layers (Dickert et al. 2003; Dickert, Lieberzeit, and Hayden 2003; Dickert et al. 2004), and site-specific immobilization of streptavidin (Tiefenauer et al. 1997).

3.5.3. Combined Langmuir-Blodgett/Molecular Assembling Method

A more advanced approach for the immobilization of antibodies for the immunosensor coatings is through the combined Langmuir-Blodgett (LB)/molecular assembling method

(Samoylov et al. 2002a, 2002b). The method includes LB deposition (Petty 1991; Pathirana et al. 1992; Barraud et al. 1993; Pathirana 1993; Vodyanoy 1994; Bykov 1996; Pathirana et al. 1996; Sukhorukov et al. 1996; Pathirana, Neely, and Vodyanoy 1998; Olsen 2000; Pathirana et al. 2000; Olsen et al. 2003; Petrenko, Vodyanoy, and Sykora 2007; Olsen 2005; Olsen et al. 2007) of a biotinylated monolayer onto a sensor surface and non-LB, molecular self-assembling of a probe layer using biotin/streptavidin coupling (Furch et al. 1996; Volker and Siegmund 1997).

The combined LB/molecular assembling method has been demonstrated with biosensors based on phage display-derived peptides as biorecognition molecules (Samoylov et al. 2002a, 2002b). Schematic design of the peptide sensor is shown in Fig. 12.8a. Monolayers

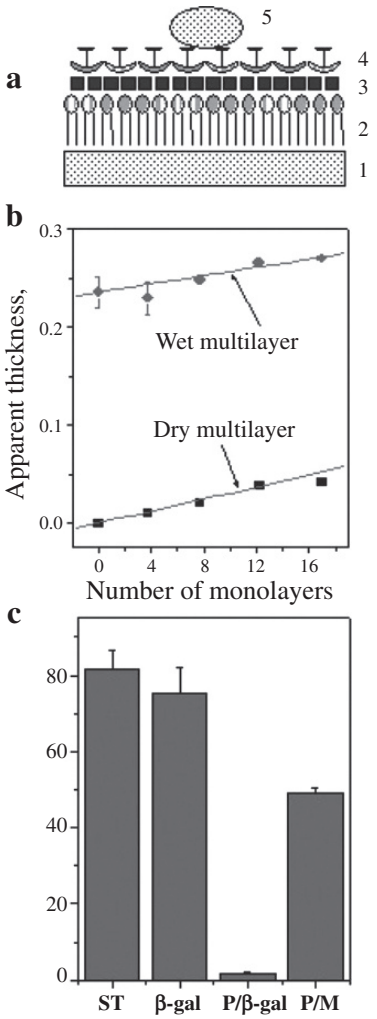

Figure 12.8. Design and functional validation of a peptide biosensor. (a) The schematic design of the peptide biosensor. The biosensor consists of four components: 1 - quartz crystal; 2 - biotinylated phospholipid; 3 - streptavidin; 4 - biotinylated peptide; 5 is a tissue vesicle. (b) Calibration of acoustic wave device with stearic acid monolayers. (c) Validation of peptide sensor preparation. **ST** – sensor was covered with biotinylated phospholipid and exposed to streptavidin. The bar represents the change of mass due to binding of streptavidin to biotinylated phospholipid. **β-gal** – sensor covered with streptavidin was exposed to β-gal solution. The bar represents the change of mass due to binding of β-gal to streptavidin. **P/β-gal –** completed sensor, covered with peptide, was exposed to β-gal. The bar represents the change of mass due to β-gal binding to the sensor. **P/M-** completed sensor, covered with peptide, was exposed to murine muscle homogenate. The bar represents the change of mass due to binding of the component of the tissue homogenate (3.8 mg/ml protein) to the peptide. (Samoylov et al. 2002b. © John Wiley & Sons Limited. Reproduced with permission).

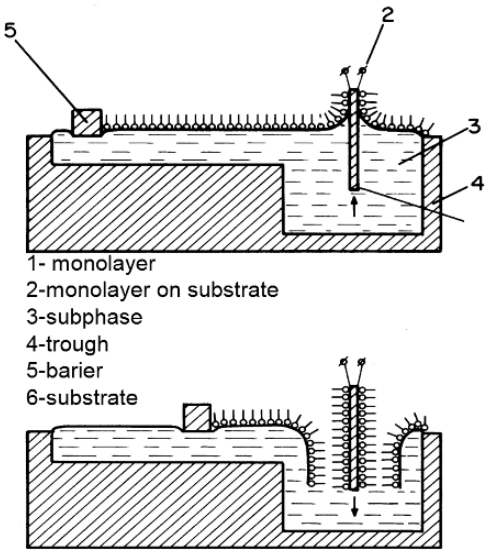

Figure 12.9. Langmuir-Blodgett (LB) monolayers. First, a monolayer is formed on a subphase surface and compressed to a desired surface pressure. A solid substrate is then moved through the monolayer vertically, so that it is dipped into and withdrawn completely out of subphase. The first monolayer is transferred to the substrate like a carpet with the tail groups toward the substrate surface during the downward movement of the substrate through the condensed monolayer. A monolayer is transferred to the substrate both when it is raised through and when it is lowered into the subphase through a compressed monolayer (reprinted from Yilma et al. (2007), with permission of Elsevier).

containing phospholipid, N-(biotinoyl)-1,2-dihexadecanoyl-sn-glycero-3-phosphoethanolamine (2), were transferred onto the gold surface of an acoustic wave sensor (1) using the Langmuir–Blodgett technique. Multilayers were obtained by successive dipping of the sensors through the monomolecular film deposited at a water-air interface (Fig. 12.9). Biotinylated peptide (4) was coupled with the phospholipid via streptavidin intermediates (3) by molecular self-assembly. Measurements of binding of target vesicles were carried out using a PM-700 Maxtek plating monitor with a frequency resolution of 0.5 Hz at 5 MHz. The device was calibrated with stearic acid monolayers. The deposition of increasing numbers of stearic acid monolayers on the surface of acoustic wave crystal resulted in linear increase of the mass (Fig 12.8b). The deposition of a single monolayer of stearic acid on the crystal resulted in additional mass of $2.6 \times 10^{-7}\,\mathrm{g\,cm^{-2}}$. This agrees well with the theoretical estimate based on the molecular area of stearic monolayer in the condensed state (Davies and Rideal 1963). Binding of streptavidin to biotinylated phospholipid is an important step in immobilization because concentration and orientation of streptavidin molecules determine the properties of a bound molecular probe. The change of mass due to streptavidin binding normally reached $80\,\mathrm{ng\,cm^{-2}}$, or $8 \times 10^{11}\,\mathrm{molecules\,cm^{-2}}$ (Fig. 12.8c—ST). When the samples were exposed to 500 nM biotinylated β-gal for 2 h the apparent mass change was at the level of $80\,\mathrm{ng\,cm^{-2}}$, or $3.4 \times 10^{11}\,\mathrm{molecules\,cm^{-2}}$ (Fig. 12.8c—β-gal). The completed biosensor, covered with the biotinylated peptide, no longer bound biotinylated β-gal (Fig. 12.8c—P/ β-gal), but strongly bound target vesicles (Fig. 12.8c—P/M).

The combined LB/molecular assembling method was also exercised in the immobilization of filamentous phage onto the surface of thickness shear mode (TSM) quartz sensors (Petrenko et al. 2005; Olsen et al. 2006, 2007). Monolayers containing biotinylated phospholipid were transferred onto the gold surface of the sensor using the Langmuir-Blodgett technique (Fig. 12.9). Biotinylated phage was coupled with the phospholipid via streptavidin intermediates by molecular self-assembling. The dissociation constant of 0.6 nM found by this method compares well with one found for antibodies isolated from a phage display library (Vaughan et al. 1996).

3.5.4. Solvent-Free Purified Monolayers

An important aspect of sensor preparation is defining the conditions under which monolayers prepared with bioreceptors can be successfully formed on a liquid/gas interface and then optimized in terms of sensitivity, reliability, and useful lifetime. Although some effects of pH, ionic strength, and oriented coupling on the immunosensor performance have been examined (Barraud et al. 1993; Ahmad and Ahmad 1996), detailed information about the influence of physical, chemical, and molecular environments on the antigen-antibody system remains largely unknown.

Traditional methods for forming LB films (Gaines 1966) require dissolution of monolayer forming compounds into a volatile organic solvent. As a separate phase, the organic solvent functions to prevent dissolution of the monolayer components in the aqueous phase. When the mixture is spread onto an aqueous subphase solution at the air-liquid interface, the solvent evaporates, leaving a monolayer at the interface. Unfortunately, the organic solvent often damages the monolayer components and leaves an undesirable residue (Sykora, Neely, and Vodyanoy 2004). LB films formed from such monolayers may also possess unacceptable levels of nonspecific binding (Ahluwalia et al. 1992), which is non-saturable and hampers quantitative measurement of specific binding. These problems can be solved using methods of monolayer formation that don't require use of an organic solvent (Trurnit 1960; Sobotka and Trurnit 1961; Pattus, Desnuelle, and Verger 1978; Pattus and Rothen 1981; Pattus et al. 1981) and have been demonstrated by immobilizing polyvalent somatic O antibodies specific for most *Salmonella* serovars onto gold electrodes of TSM resonators using the LB method (Pathirana et al. 2000).

Many features of antibody immobilization originate from the very nature of the antibody itself. Typical antibodies are Y-shaped molecules (2 Fab plus Fc immunoglobulin structure) with two antigen binding sites located on the variable region of the Fab fragments. All classes of antibody produced by B lymphocytes can be made in a membrane-bound form and in a soluble secreted form (Alberts et al. 1994). The two forms differ only in their carboxyl terminals; the membrane-bound form has a hydrophobic tail (Fc) that anchors it in the lipid bilayer of the B cell membrane, whereas the secreted form has a hydrophilic tail, which allows it to escape from the cell. Of these, only the form with a hydrophobic tail is capable of being held by the monolayers. Thus, it is uniquely qualified for use in the Langmuir-Blodgett technique. This form also renders it suitable for proper alignment and orientation in sensor membranes.

Antibodies derived from immunized animals in the form of antisera or purified protein preparations can be present in both membrane-bound and soluble form and may contain impurities. Organic solvents used as a spreading carrier in LB monolayer preparation may drag these impurities and both forms of antibodies into the monolayer. Furthermore, these methods may produce monolayers with high densities of antibodies but also with residuals of organic solvent, impurities, and entrapped hydrophilic antibodies that destabilize the monolayer and modulate antigen-antibody interactions. A monolayer with no solvent can be formed on the air-liquid interface by allowing the spreading solution to run down an inclined wetted planar surface that is partially submersed into subphase (Fig. 12.10) (Pathirana et al. 2000). Membrane vesicles (natural components of serum, or the artificial lipid vesicles) are positioned on a wet slide at the edge of a positive meniscus of liquid, at the liquid-air interface. The hydrophobic antibodies are bound to the vesicular membrane; hydrophilic antibodies and some impurities are suspended inside the vesicle. When surface forces rupture the vesicle, it splits into a monolayer and purification occurs. Membrane-bound antibodies are left bound to the newly created monolayer, but soluble antibodies and impurities dissipate into the subphase beneath the monolayer. Only membrane-bound antibodies surrounded by compatible lipids are left when the monolayer is compressed and transferred onto a sensor surface. Alternatively, probes can be conjugated with vesicles by covalent binding (Betageri et al. 1993). Lipid vesicles containing whole antibodies or Fab fragments can also be constructed. Large, unilamellar liposomes

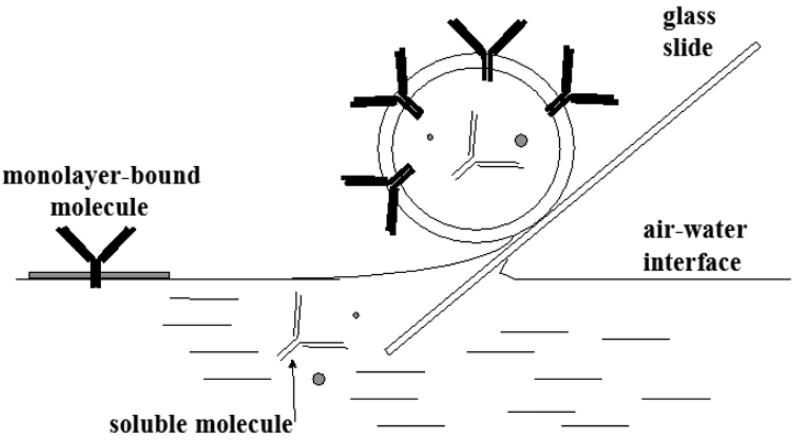

Figure 12.10. Monolayer formation from lipid vesicles. Surface forces rupture the vesicle, splitting it into a monolayer. The monolayer, with the membrane-bound molecules, is then compressed and transferred onto the sensor surface (reprinted from Pathirana et al. (2000), with permission of Elsevier).

are prepared from synthetic L-α(1,2-dipalmitoyl-sn-glycero-3-phosphocholine) (DPPC) and maleimido phenyl butyrate phosphatidylethanolamine (MPB-PE). Monoclonal antibodies (or Fabs) with specificity for *S. typhimurium* or *E. coli* O157:H7 are modified by the heterobifunctional reagent N-Succinimydyl-3(2-pyridyldithio)propionate (SPDP) in the presence of dicetyl phosphate and dithiothreitol (DTT) and conjugated to liposomes. The liposomes, containing specific antibodies, are then converted into monolayers and deposited on the sensor surface by the LB method (unpublished results).

3.5.5. Immobilization of Monolayers of Phage Coat Proteins

3.5.5.1. Phages As a Recognition Probe

A large number of bio-assays and biosensors depend on highly specialized, sensitive, and selective antibodies as recognition reagents (Goodchild et al. 2006). While antibodies frequently have the desired sensitivity and selectivity, their use is limited by many factors. For example, the binding properties of antibodies may be lost due to unfavorable environmental conditions (Olsen et al. 2003). This factor can be especially important in dealing with environmental applications, where organic solvents must be used for extraction of compounds (Ahmad and Ahmad 1996). Also, production of polyclonal antibodies requires a process that is very time- and labor-intensive, and can produce a variable product. Production of monoclonal antibodies is often even more difficult and expensive. These limitations can be addressed in part by using bacteriophage or their coat proteins as recognition elements for biosensors (Goldman et al. 2000; Petrenko et al. 2005; Nanduri et al. 2007). Both lytic and filamentous phages present reach libraries to identify proteins interacting with molecular targets. In phage display, the phage filament serves as the framework for random peptides that are fused to the N-terminus of every copy of the major phage coat protein. These random peptides form the "active site" of the landscape phage and comprise up to 25% by weight of the particle and up to 50% of its surface area (an extraordinarily high fraction compared with natural proteins, including antibodies) (Nanduri et al. 2007). A large mixture of such phages, displaying up to a billion different guest peptides, is called a "landscape library." From this library, phages can be affinity selected for specificity to a certain antigen, thus functionally mimicking antibodies. These phages can be efficiently and conveniently produced and are secreted from the cell nearly free of intracellular

components in a yield of about 20 mg/ml (Nanduri et al. 2007). The purification procedure is simple and does not differ dramatically from one clone to another. The surface density of the phage binding peptides is 300–400 m^2/g, comparable to the best known absorbents and catalysts (Nanduri et al. 2007), and with thousands of potential binding sites per particle, creates a multivalency. Other advantages of phages over antibodies include the extraordinary robustness of the phage particle. It is resistant to heat (up to 70 °C), many organic solvents (such as acetonitrile), urea (up to 6M), acid, alkali, and many other stresses (Nanduri et al. 2007). Purified phages can be stored indefinitely at moderate temperatures without losing infectivity (Nanduri et al. 2007). Thus, phages may be viable as substitute antibodies in many applications such as biosensors, affinity sorbents, hemostatics, etc. Numerous examples of uses of both lytic and filamentous phages as probes for biological detection in biosensors have been reported in the literature (Chin et al. 1996; Ramirez et al. 1999; Goldman et al. 2000, 2002; Auner et al. 2003; Olsen et al. 2003; Sayler, Ripp, and Applegate 2003; Ozen et al. 2004; Petrenko, Vodyanoy, and Sykora 2007; Tabacco, Qian, and Russo 2004; Chen et al. 2005; Nanduri 2005; Petrenko et al. 2005; Sorokulova et al. 2005; Wu et al. 2005; Lakshmanan et al. 2006; Olsen et al. 2006; Balasubramanian et al. 2007; Nanduri et al. 2007).

3.5.5.2. Phage Coat Technology

A critical step in the use of whole phages or phage proteins as a bioreceptor is their immobilization to the platform area on the sensor where the analytes (bacteria, toxins, etc.) will bind. Immobilization of whole phage particles to a sensor surface presents certain difficulties with phage positioning. While multivalent, phage particles are typically assembled in bundles that may present obscurity of binding sites (Fig. 12.11). Immobilization of proteins extracted by organic solvents may present difficulties in depositing a correctly orientated layer of proteins on the sensor surface. A better way of phage protein immobilization is to use the intact protein coat of the phage particle. For example, when T2 lytic bacteriophage was subjected to osmotic shock, it lost most of its DNA, but the protein coat or "ghost" of the phage was left intact (Herriott and Barlow 1957). The coat retained the phage shape and some of the biological functions of the phage. Kleinschmidt and coworkers (Kleinschmidt et al. 1962) were able to

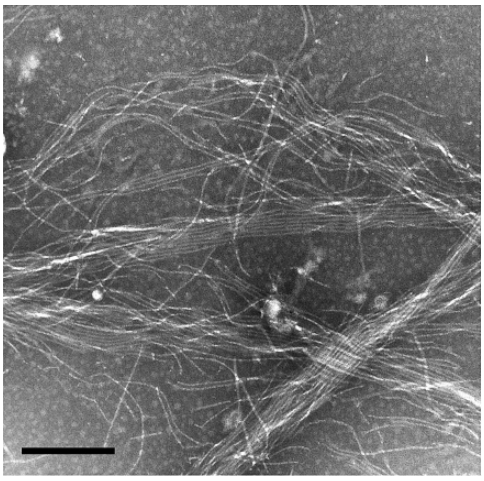

Figure 12.11. Transmission electron micrograph of bacteriophage 1G40 on a formvar, carbon coated grid of 300 mesh size using a wetting agent (0.1% BSA). The phage particles have aggregated as bundles on the grid. Bar = 200 nm (courtesy of Dr. V. Nandury).

convert T2 coat particles into protein monolayers by allowing the water suspension of coat particles to run down a wet glass rod glass surface that was partially submersed into subphase (similar to that shown in Fig. 12.10) (Trurnit 1960; Sobotka and Trurnit 1961; Pattus, Desnuelle, and Verger 1978; Pattus and Rothen 1981; Pathirana et al. 2000).

Monolayers made of the phage coats transferred to solid substrates were first described by Kleinschmidt et al. (1962). A similar approach was applied to obtain monolayers of filamentous phages. Griffith and coworkers (Griffith, Manning, and Dunn 1981; Petrenko, Vodyanoy, and Sykora 2007; Olsen 2005) demonstrated that filamentous bacteriophages transformed into hollow spherical particles upon exposure to a chloroform-water interface. These particles could then be converted into monolayers and deposited onto solid substrate by the LB method (Sykora 2003; Olsen 2005). Thus, the technology of phage coat immobilization consists of three major steps: phages are first converted into spheroids, monolayers are formed from the spheroids, and finally the monolayers are deposited onto the sensor surface by the LB method.

Phage coat monolayers made of coats of lytic and filamentous phages have been immobilized onto biosensor surfaces. When a suspension of filamentous phage protein streptavidin binder, 7b1, (Petrenko and Smith 2000) was vortexed with an equal volume of chloroform and the aqueous phase was examined by electron microscopy, spherical particles termed "spheroids" were observed along with other semicircular particles that may be intermediates in the filament to spheroid conversion (Griffith, Manning, and Dunn 1981).

Chloroform transforms the infectious phage filaments into non-infective hollow spheres. This drastically alters the surface architecture of the phage. As well, the α-helix content of pVIII decreases from 90% to 50–60% (Griffith, Manning, and Dunn 1981; Roberts and Dunker 1993). Spheroids are formed when the coat proteins contract into vesicle-like structures and two-thirds of the phage DNA is extruded (Griffith, Manning, and Dunn 1981). An electron micrograph of this is shown in Fig. 12.12 (Petrenko, Vodyanoy, and Sykora 2007). Similar hollow spheroids can be obtained by the same method from phage f8–1 that bind *Salmonella typhimurium* (Olsen 2005). Olsen formed LB monolayers from the spheroid suspension using a wetted glass rod that was partially submersed into the subphase (Trurnit 1960; Sobotka and Trurnit 1961; Kleinschmidt et al. 1962; Pattus and Rothen 1981; Pathirana et al. 2000; Petrenko, Vodyanoy, and Sykora 2007; Olsen 2005). After the vesicle slid down the glass rod and reached the air-water interface, surface forces ruptured the vesicle and split it into a monolayer.

Compression of an LB monolayer prepared from a spheroid suspension yields a pressure (Π)-area (A) isotherm (Fig. 12.13) (Sykora 2003). The curve is biphasic, having a small "kink"

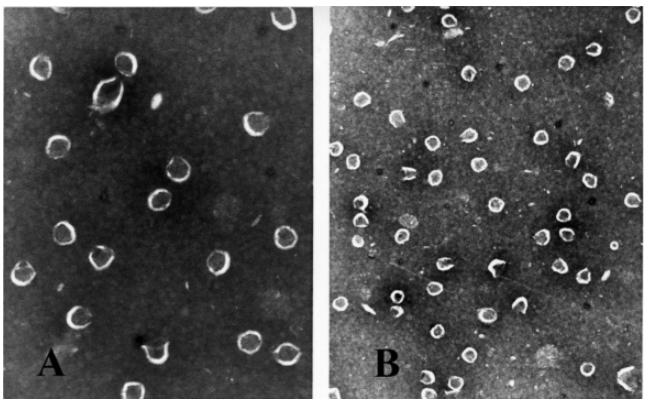

Figure 12.12. Electron micrographs of 7b1 filamentous bacteriophage following chloroform treatment. Sample was stained with 2% phosphotungistic acid. Spherical particles are called "spheroids." Mag., 302,500x (A) and 195,300x (B) (Olsen et al. 2007; reproduced by permission of The Electrochemical Society).

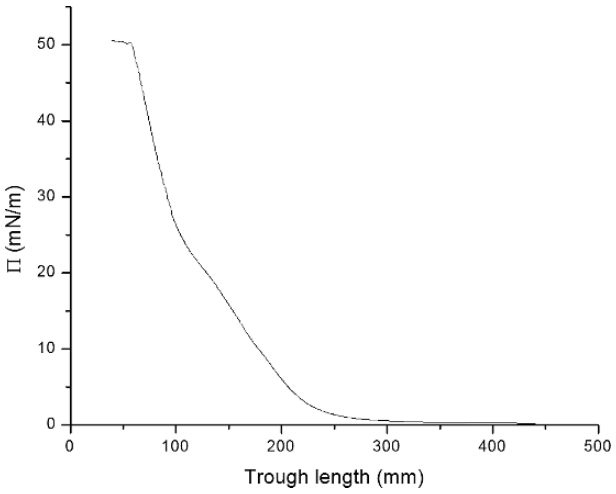

Figure 12.13. Surface pressure-area isotherm of monolayer formed when 7b1 spheroid suspension was spread at the air/water interface at 21 °C and compressed at a rate of 30 mm/min.

around 20 mN/m, followed by a steep condensed region. A pressure of $\sim 50\,\mathrm{mN/m}$ was noted before the barrier reached the end of its stroke. This pressure is very high for protein monolayers, indicating a very stable system (Davies and Rideal 1963; Gaines 1966). Fig. 12.14 shows elasticity versus surface pressure for the monolayer. There are two maxima in elasticity separated by a minimum around 20 mN/m (from the "kink" in the isotherm). The largest maximum reach was $\sim 50\,\mathrm{mN/m}$, very high for protein monolayers (Davies and Rideal 1963; Gaines 1966), at a pressure of 30 mN/m. This pressure is optimal for transferring monolayers onto solid sensor substrates by the LB method (Petrenko, Vodyanoy, and Sykora 2007). A similar technology for immobilization of a *Salmonella* binder phage E2 onto a surface of a QCM sensor was developed by Olsen et al. (2007).

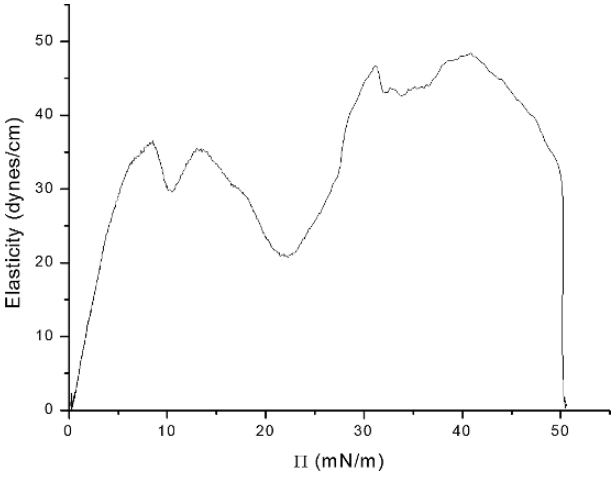

Figure 12.14. Graph of elasticity versus surface pressure (Π) for monolayer formed from spreading of spheroid suspension. Elasticity was calculated from the surface pressure-area isotherm (Fig. 8.13).

3.5.5.3. Phage Coat Protein Structure

The amino acid sequence of the pVIII coat protein from phage 7b1 with the foreign octapeptide insert is shown in Fig. 12.15. Conformation of the pVIII binding peptide at both the air/water interface and on the sensor surface can be elucidated based on the amino acid sequence. The octapeptide insert consisting of residues number 2 through 9 is located at the N-terminal region. Based on the amino acid sequence, the peptide is expected to have three α-helical regions according to both the Garnier-Robson (Garnier, Osguthorpe, and Robson 1978) and Chou-Fasman (Chou and Fasman 1974) calculation methods, as shown in Fig. 12.16. The central region of the peptide is hydrophobic, while the N-terminal and C-terminal regions are somewhat hydrophilic. This hydrophobic region is the part of the peptide that spans the bacterial cell membrane during assembly (Bashtovyy et al. 2001; Houbiers et al. 2001; Branch and Brozik 2004; Houbiers and Hemminga 2004; Aisenbrey et al. 2006). Most of the amphipathic and flexible regions of the peptides correspond with the hydrophilic regions of the peptide. According to calculations of the antigenic index, the most probable antigen-binding region lies on the N-terminus, which is the region where the octapeptide insert is located.

A hypothetical arrangement of the pVIII coat proteins at the air/water interface is shown in Fig. 12.17. Here, the hydrophilic N-terminal and C-terminal α-helices interact with the water phase while the central hydrophobic region remains at the interface. A hypothetical arrangement of these peptides on the sensor surface is subsequently shown in Fig. 12.18 (Bashtovyy et al. 2001; Houbiers et al. 2001; Houbiers and Hemminga 2004; Im and Brooks 2004; Aisenbrey et al. 2006). Here the peptides are suggested to be arranged in a conformation similar to that

N-AVPEGAFSSDPAKAAFDSLQASATEYIGYAWAMVVVIVGATIGIKLFKKFTSKAS-C
1 2

Figure 12.15. Amino acid sequence of 7b1 filamentous bacteriophage pVIII coat protein. The foreign octapeptide insert, VPEGAFSS (underlined region 1), is located between residues 1 and 10 at the N-terminal portion (N) of the protein. The hydrophobic region of the protein is underlined. C designates the C-terminus of the peptide.

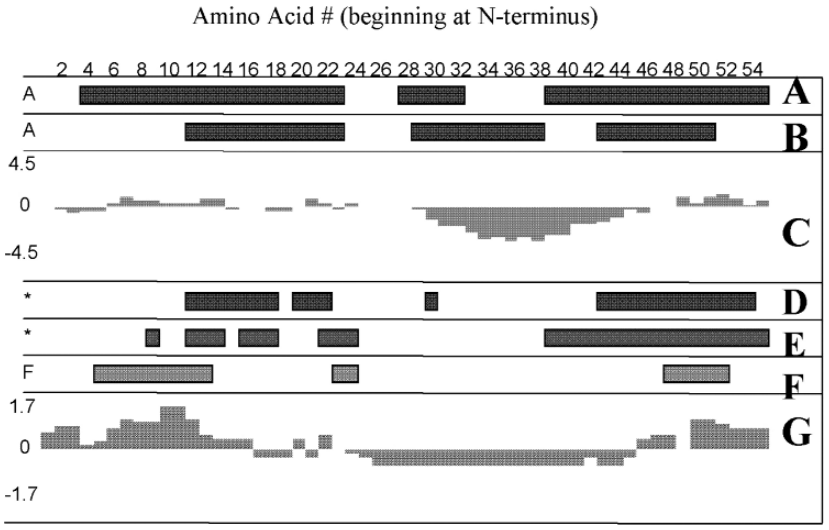

Figure 12.16. DNASTAR analysis of pVIII phage coat protein: (A) α-helical regions (Garnier-Robson method); (B) α-helical regions (Chou-Fasman method); (C) hydrophilicity plot; (D) α-helical amphipathic regions; (E) β-sheet amphipathic regions; (F) flexible regions; (G) antigenic index. (Olsen et al. 2007; reproduced by permission of The Electrochemical Society).

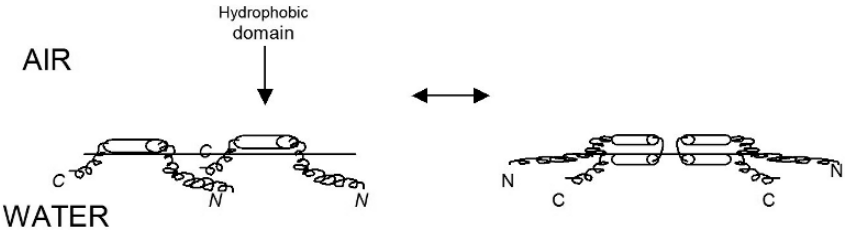

Figure 12.17. Hypothetical schematic of the arrangement of pVIII coat proteins at the air/water interface. N and C designate the N-terminus and C-terminus of the peptide, respectively, while the cylinder represents the hydrophobic domain. (Olsen et al. 2007; reproduced by permission of The Electrochemical Society).

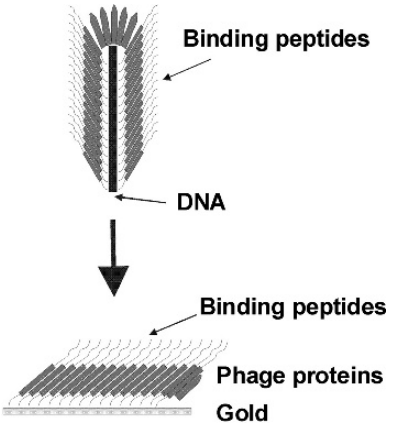

Figure 12.18. Hypothetical arrangement of skinned phage deposited to hydrophilic QCM substrates by Langmuir-Blodgett method. (Olsen et al. 2007; reproduced by permission of The Electrochemical Society).

in the phage particle, where the positively charged lysine residues of the C-terminal region interact with the negatively charged gold surface, thus allowing the N-terminal region and the octapeptide insert to be exposed to solvent.

3.5.6. Immobilization of Molecular Probes onto Porous Substrates

Immobilization of large molecular probes (antibodies, proteins, DNA, etc.) requires a complex environment in order to maintain viability and functional activity of the probes. These conditions are difficult to meet on a continuous solid sensor surface. Under natural conditions biological receptors are supported by biological membranes that are interfaced with water solutions on both sides. The Australian group of Cornell (Cornell et al. 1997, 2001) devised a multi-step assembly procedure to tether a lipid bilayer containing molecular probes linked to a gold surface. Such a tethered configuration is of interest in general for sensor technology because it creates a water reservoir between the sensor surface and membrane and serves to maintain the bilayer fluidity and facilitate the incorporation of molecular probes. Although this example clearly demonstrates the feasibility of an electrode-supported ion channel-based sensor, it suffers from several serious problems. First is the shear complexity of the synthetic approach; using thiol- and lipid-based self-assembly techniques, six different reagents are sequentially organized onto the gold surface. Second, because the tethers are randomly positioned on the electrode, weaker unsupported regions of the membrane could collapse. Finally, there appears to be no obvious patterning procedure. To overcome the above problems and in addition develop

qualitatively new functionalities, thin porous substrates of silica have been developed (Fan et al. 2000; Jiang et al. 2006; Nishiyama et al. 2006; Xomeritakis et al. 2007). These films can be used as a new type of support for molecular probes in biosensors (Thust et al. 1999; Bessueille et al. 2005; Gawrisch et al. 2005; Yun et al. 2005; Dai, Baker, and Bruening 2006; Song et al. 2006). In our laboratory we have immobilized the antimycotic agent amphotericin B onto the porous silicon surface and observed ion currents associated with ion conductance of amphotericin B ion channels connected to internal and external reservoirs of liquids separated by a membrane (Yilma et al. 2007a, 2007b).

4. Problem of "Negative Mass"

The thickness shear mode quartz crystal resonator (QCM) is often considered a mass-sensitive sensor. During the sensing process, it's expected that the response (frequency change, Δf) of the sensor is directly related to any additional mass that adheres to the resonator, usually resulting in a resonance frequency decrease ($\Delta f < 0$). Sauerbrey (1959) demonstrated this for thin, rigid layers (like metal film). For mass m the frequency decrease is

$$\Delta f = -f_0 \frac{\Delta m}{M_q},$$

where, f_0 is the resonance frequency and M_q is the mass of a quartz oscillator. However, use of QCM for in situ bacteria and cell detection in fluids has revealed more complex sensor responses. For example, the observed value of Δf differs from that predicted by Sauerbrey's (1959) relation, and the signal is often small (Thompson et al. 1991; Voinova, Jonson, and Kasemo 2002).

Observed deviations from Sauerbrey's (1959) predicted mass theory have been noted during sensor testing under liquid conditions using both antibodies (Olsen et al. 2003) and phages (Olsen et al. 2006) as bioreceptors. The most peculiar results show that under certain conditions there is an appearance of a negative apparent mass; i.e., with increasing bacterial concentration there can be a dose-dependent decrease of the apparent mass. It is possible that the bacterial microenvironment and location of the antigen on the surface of a bacterium can determine the value and sign of the analytical signal generated by the acoustic wave device (Olsen et al. 2003). Bacterial positioning and binding may be very important at the solid/liquid interface of the sensor and factors such as viscoelasticity, shear forces and damping. For example, in our studies using *Salmonella* and *E. coli* antibodies as receptors (Olsen et al. 2003), when attachment between bacteria and bacteria-specific somatic O antibodies at the solid-liquid interface of a TSM resonator was rigid and strong, the sensor's output was directly proportional to the logarithmic concentration of free bacteria in suspension, and the sensor's behavior could be described as that predicted by mass theory ($\Delta f < 0$) (Fig. 12.19a). Conversely, flexible binding observed for bacteria attached by flagella to immobilized flagellar H antibodies resulted in inversely proportional sensor signals ($\Delta f > 0$) (Fig. 12.19b). This premise was affirmed by studying the responses of environmentally aged sensors. Sensor responses and binding efficiency, confirmed by dark-field microscopy, decreased as the duration of sensor environmental aging under differing conditions of temperature increased (Fig. 12.20).

Viscoelastic properties of the bacterial layer attached to the surface are anticipated to be different depending on the mechanism of binding—somatic or flagellar. Also, the viscous shear and viscous drag forces of the attached bacteria are very different. Clearly, bacteria rigidly or flexibly attached (Fig. 12.21) take different roles in the oscillation of the whole system. When binding is rigid, bacteria oscillate in unison with the sensor and therefore contribute to the effective oscillating mass of the system. This is shown by the increase of the apparent

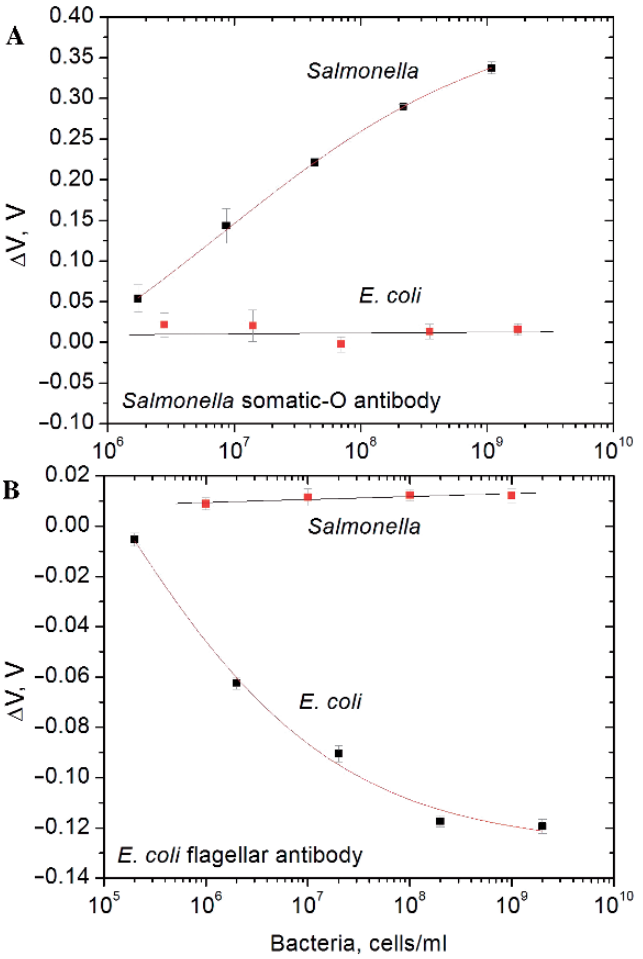

Figure 12.19. Dose responses for rigid and flexible positioning of bacteria on biosensor: (A) *Salmonella* and *E. coli* dose responses to sensor prepared with somatic O *Salmonella* antibodies; (B) *Salmonella* and *E. coli* dose responses to sensor fabricated with flagellar H-type *E. coli* antibodies. Curves are sigmoid fit to experimental data. Straight lines are the linear least squares fit. Bars are SD (reprinted from Olsen et al. (2003), with permission of Elsevier).

mass when bacterial binding concentration is increased. Conversely, in the case of flexible attachment, the oscillation of the bacteria may be not in phase with the oscillation of the sensor, resulting in a decrease in the apparent mass even when concentration of binding bacteria is increased. Additionally, we propose that the electrically charged bacterium on the surface of an acoustic wave sensor is not only engaged in the mechanical oscillations of the crystal but also directly interacts with the electric field driving the sensor crystal. This field drives the piezoelectric quartz crystal and at the same time creates an electrophoretic force applied to the electrically charged bacterium. The piezoelectric and electrophoretic forces can be of different values and directions, depending on the positioning of bacteria by the O antigen (Fig. 12.21a—firm positioning) or the H antigen (Fig. 12.21a—flexible attachment), and their combination may contribute to the change of the apparent mass of the bacteria as measured by the acoustic wave device. Obstruction of antibodies by the buildup of a biofilm during aging may cause decreased accessibility to bacterial targets (Fig. 12.21a—weak binding).

In contrast with Sauerbrey's (1959) observations for a thin, firmly attached film, this seeming contradiction of normal mass loading theory is consistent with the observations of

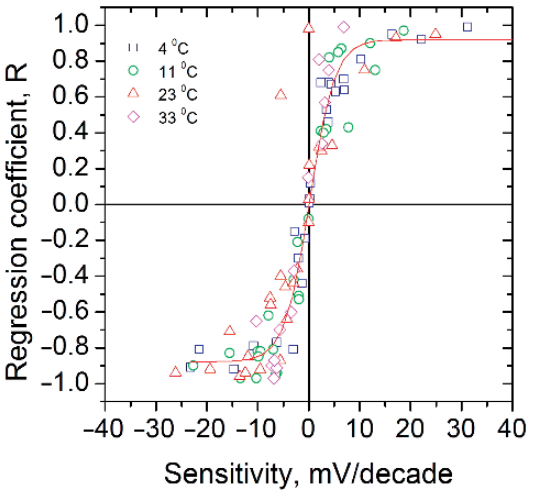

Figure 12.20. Experimental regression coefficient of individual sensors (e.g., see Fig. 12.3b) at differing temperatures as a function of sensitivity for environmentally aged *Salmonella* sensors prepared with somatic O antibodies. The linear portions of dose response signals were fitted by linear regression. Curve is the sigmoidal fit to experimental data points at indicated temperatures (reprinted from Olsen et al. (2003), with permission of Elsevier).

Dybwad (1985), who first described mass-dependent frequency increases in conjunction with particulates, such as small (10–50 μm diameter) Au spheres, under normal atmospheric conditions while loosely attached to a horizontally positioned QCM resonator. Dybwad's (1985) proposed equivalent mechanical model (Fig 12.21b) of a loosely bound particle as a coupled mass-spring system corresponds exactly with the flexible attachment of our simplified model shown in Fig. 12.21a (Olsen et al. 2003) depicting bacterial positioning at the sensor surface as the determinant factor of the sensor's analytical response. Dybwad's (1985) results were affirmed by Vig and Ballato (1998), who stated:

> "Significant deviation from the Sauerbrey equation will also occur when the mass is not rigidly coupled to the QCM surfaces. The effects of liquids have been discussed in the sensor literature [references given]; however, the effects of nonrigid coupling of solids do not seem to be well-

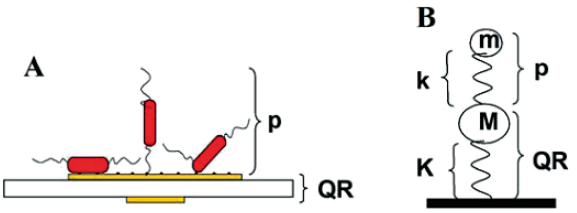

Figure 12.21. Mechanical models of analyte-resonator interaction as composite and coupled oscillators. (A) Corresponding model of Olsen et al. (2003) that shows bacterial binding positions (p) at the solid/liquid interface of the quartz resonator (QR). When binding is firm between bacteria and receptor (left), the natural frequency of the cell as an independent mass-spring system equals the frequency of the resonator, forming a composite unit that produces expected mass loading effect with corresponding frequency decrease. When binding is flexible or weak (center and right, respectively) between analyte and receptor a coupled oscillator is formed, the frequency of which is dictated by the difference in the spring constants between the oscillator and bacteria. (B) Coupled oscillator model of Dybwad (1985) depicting quartz resonator (QR) as one mass (M) spring (K) system, and a loosely attached particle (p) as a second mass (m) spring (k) system. Attachment of the loose particle causes QR to oscillate at a new, higher frequency when $k < K$. When $k = K$, a composite system is formed that produces expected mass loading effect with corresponding frequency decrease.

known. For example, when a particle is placed on an electrode of a QCM, the Sauerbrey equation predicts a decrease in the frequency of the QCM, but the frequency actually increases. When the particle on the resonator is modeled as a coupled oscillator, the model correctly predicts a frequency increase [as verified by Dybwad (1985)]."

This type of behavior has been documented in the literature on several occasions. Berg, Johannsmann, and Ruths (2002) used a single asperity contact to show that frequency shifts associated with a quartz resonator operating in shear mode increased linearly with increasing contact radius. Borovsky et al. (2001) used a nanoindenter probe in conjunction with a QCM to elicit positive frequency shifts characteristic of the contact stiffness. Sorial and Lec (2004) experienced size-dependent frequency increases with polystyrene spheres using a QCM under aqueous conditions. Otto et al. (1999) observed diminished, $\Delta f < 0$, response for weaker bacteria attachment using an *E. Coli* QCM sensor. Other documented reports of negative apparent mass using QCM-based platforms include Hayden et al. (2003) and Dickert et al. (2003), in response to loose binding of bacterial cells in yeast imprinted layers; Dickert et al. (2004), due to loose binding of non-specific compounds to tobacco mosaic virus imprinted polymers; Marxer et al. (2003), who attributed frequency increases to alterations in cytosolic viscosity of adsorbed epithelial cells; Thompson, Arthur, and Dhaliwal (1986), due to immunochemical interactions resulting in decreased acoustic transmission at the liquid/solid interface; and Pereira de Jesus, Naves, and Lucia do Lago (2002), as a result of polymeric film stiffness in the determination of boron. More recently, Lucklum (2005) described non-gravimetric contributions of viscoelastic films at the solid/liquid interface, resulting in positive frequency shifts. He clearly showed that typical elastic and energy dissipation properties are as important to frequency response, both positive and negative, as the layer's mass and therefore in many cases the added mass cannot be determined simply from the QCM response alone. The author correctly notes that the traditional name "quartz crystal microbalance (QCM)" as a technique is misleading.

Collectively, these reports support our hypothesis that positive frequency shifts can be observed under certain conditions as a result of viscoelastic changes at the solid/liquid interface from surface films, bioreceptor layers, and bacterial attachment. We contend that the continuous model of the viscoelastic layer is not directly applicable to the bacterial sensing. This is a consideration for researchers in terms of the importance of bacterial attachment schemes (bioreceptors) that result in high-affinity and multiple binding valences. In the next section, we present a coupled oscillators model that explicitly accounts for discrete events of bacteria attachment in terms of the elastic constant and the dissipation of the bond between bacteria and the sensor surface. This model is in agreement with our previous model (Olsen et al. 2003), since the parameters of an LRC series equivalent circuit model of the QCM are perfectly analogous to a damped harmonic oscillator system (Table 12.5).

Table 12.5. Analogous parameters between a mechanical spring-mass system and LRC series circuit

		System	
Harmonic Oscillator	Unit	LRC Circuit	Unit
Displacement	x	Charge	q
Velocity	v	Current	I
Force	F	Voltage	V
Mass	m	Inductance	L
Damping constant	b	Resistance	R
Spring constant	k	Capacitance^{-1}	1/C
Natural frequency	$\omega_o = (k/m)^{1/2}$	Natural frequency	$\omega_o = (1/C)^{1/2}$

5. Coupled Oscillators Model

The continuous layer model does not elucidate total understanding of the bacterial sensing process when discrete bacteria are bonded to the sensor surface. We present here a simple coupled oscillators model, depicted in Fig. 12.22.

The unloaded quartz oscillator is described by the oscillator of mass M connected to the spring with the force constant K and moving in the fluid with the viscous friction force -Γv, where v is velocity. This oscillator models realistic assay conditions where the bacterial bioreceptors (e.g., antibodies or phages) are deposited on the surface of an immersed TSM transducer, but no bacteria are present. The bonded bacterium of mass m is connected to the oscillator by an elastic bond with the force constant k and experiences a viscous friction with coefficient γ. The equations of the motion for the quartz oscillator and each of the oscillating bacteria numbered by the index i (i= 1, 2…n) are:

$$\begin{aligned} M\frac{d^2X}{dt^2} &= -KX - \Gamma\frac{dX}{dt} + \sum_{i=1}^{n} k(x_i - X - a) + F_0 e^{i\omega t} \\ m\frac{d^2x_i}{dt^2} &= -\gamma\frac{dx_i}{dt} - k(x_i - X - a). \end{aligned} \tag{12.6}$$

Here $F_0 \sin \omega t = \mathrm{Im} F_0 e^{iwt}$ is the periodic external force driving the oscillator. We want to find a stationary solution of Eqs. (12.6) when all the oscillators move with the frequency of the external force:

$$X = X_0 e^{i\omega t}, \; x_i - a = x_{i0} e^{i\omega t}. \tag{12.7}$$

Substitution of Eq. (12.7) into Eqs. (12.6) gives a system of linear algebraic equations:

$$\begin{aligned} &(-\omega^2 M + i\Gamma\omega + K)X_0 - \sum_{i=1}^{n} k(x_{i0} - X_0) = F_0 \\ &(-m\omega^2 + i\gamma\omega)x_{i0} + k(x_{i0} - X_0) = 0. \end{aligned} \tag{12.8}$$

To solve Eqs. (12.8) with respect to X_0, the variables x_{i0} are expressed as:

$$x_{i0} = \frac{kX_0}{-m\omega^2 + i\gamma\omega + k}. \tag{12.9}$$

Substitution of Eq. (12.9) into the first part of Eq. (12.8) gives:

$$X_0 = \frac{F_0[m(\omega_0{}^2 - \omega^2) + i\gamma\omega]}{[M(\Omega_0{}^2 - \omega^2) + i\omega\Gamma][m(\omega_0{}^2 - \omega^2) + i\gamma\omega] - nk(m\omega^2 - i\gamma\omega)}. \tag{12.10}$$

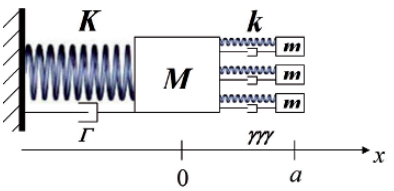

Figure 12.22. Coupled oscillator's model. Quartz resonator is presented by oscillator with mass M, spring constant K, and viscous damping Γ. Each attached bacterium is modeled as an individual coupled oscillator with mass m, spring constant k, and viscous damping γ.

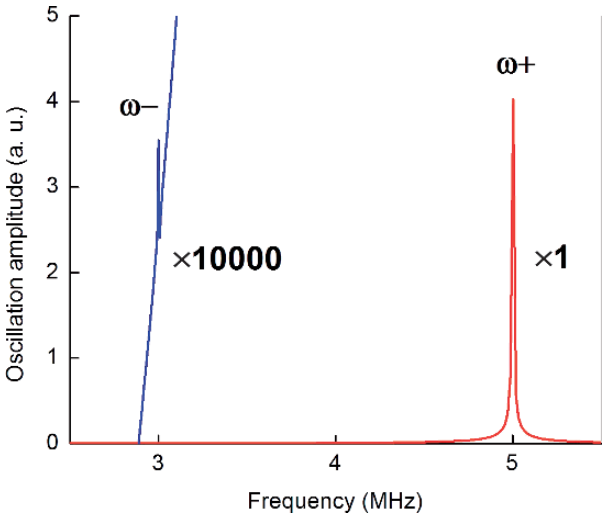

Figure 12.23. Resonance curve for the quartz resonator frequency 5 MHz and the bacteria elastic binding strength 3 MHz. Strong resonance mode ω+ (red curve) near 5 MHz is dominant where as the mode ω- (blue curve) near 3 MHz is weak (shown at 10,000X magnification).

Here,

$$\Omega_0{}^2 = K/M, \omega_0{}^2 = k/m, \tag{12.11}$$

denotes the resonance frequencies for uncoupled oscillators. The resonance frequencies of coupled oscillators correspond to maxima of the amplitude $|X_0|$ as a function of ω. Fig. 12.23 presents an example of the resonance curve for $\Omega_0/2\pi = 5 \cdot 10^6$ Hz, $\Gamma/2\pi M = 1$Hz, $\omega_0/2\pi = 3 \cdot 10^6$ Hz, $\gamma/2\pi m = 1$Hz, $n = 100$, and $m/M = 2 \cdot 10^{-7}$. As expected, the main resonance is near the quartz oscillation frequency Ω_0, because the effect of bacteria binding is small. The second weak resonance occurs near the bacterium oscillation frequency ω_0, but it is too weak to be registered experimentally.

When damping does not occur ($\Gamma = 0$, $\gamma = 0$), complete consideration of the resonances is feasible in closed analytical form. At resonance the oscillation amplitude given by Eq. (12.10) grows infinitely because the denominator is zero:

$$M(\Omega_0^2 - \omega^2)(\omega_0^2 - \omega^2) - nk\omega^2 = 0. \tag{12.12}$$

This is a square equation for ω^2 and it has two positive solutions, ω_- and ω_+. Fig. 12.24 shows ω_- and ω_+ as functions of the bacteria elastic binding strength ω_0 and $\Omega_0/2\pi = 5 \cdot 10^6$ Hz, $n = 100$, and $m/M = 2 \cdot 10^{-7}$. As discussed above and shown in Fig. 12.23, only the resonance near Ω_0 is strong and observable in a realistic case when damping occurs. Thus, in Fig. 12.24, the observable resonance corresponds to ω_+ branch when the bacteria binding is weak ($\omega_0 < \Omega_0$), but is given by ω_- branch when the binding is strong ($\omega_0 > \Omega_0$). Hence, there are two systems corresponding to the two marked rectangular areas in Fig. 12.24. First, for weak bacteria binding ($\omega_0 < \Omega_0$) the resonance frequency increases in contradiction to the intuitive expectation that the addition of the bacterial mass to the oscillator will decrease the frequency. The positive frequency shift grows when the bacteria binding ω_0 increases and approaches the frequency Ω_0. The second system corresponds to strong bacteria binding ($\omega_0 < \Omega_0$) when the resonance frequency decreases as expected for mass added to the oscillator. In this case

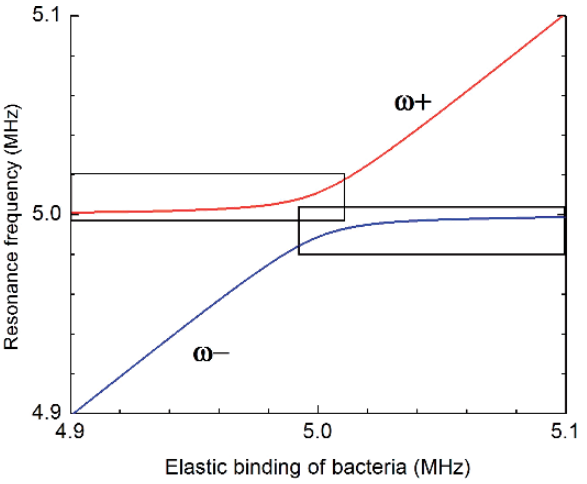

Figure 12.24. Frequency of two resonance modes ω+ and ω- as a function of the elastic binding strength of the bacteria. Each mode is strong only in the binding range denoted by the corresponding rectangle box. The mode becomes weak and finally unobservable when its frequency departs from the resonance frequency of 5 MHz.

the frequency shift becomes smaller when bacteria binding ω_0 increases. These results are also valid in the realistic case of non-zero damping ($\Gamma/2\pi M = \gamma/2\pi M = 1\,\text{Hz}$), as shown in Fig. 12.25. Again the resonance frequency shift is positive for weak and negative for strong bacterial elastic binding.

The different behavior for weak and strong bacterial attachment can be understood from the bacterial oscillator equations of motion. We evaluate Eq. (12.9) at the frequency Ω_0

$$x_{i0} = \frac{X_0}{\left(1 - \dfrac{\Omega_0^2}{\omega_0^2}\right)^2 + \dfrac{\gamma^2\Omega_0^2}{k^2}} \left(1 - \frac{\Omega_0^2}{\omega_0^2} - i\frac{\gamma\Omega_0}{k}\right). \tag{12.13}$$

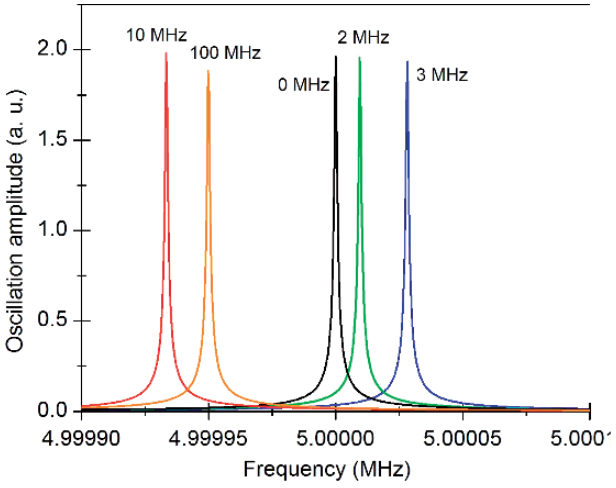

Figure 12.25. Resonance curves for different bacteria elastic binding strengths at 0 (no binding), 2, 3, 10, and 100 MHz, as noted. Notice that the shift of resonance frequency changes from negative to positive as the binding decreases below the resonance frequency of 5 MHz.

The relative phase of x_{i0} with respect to X_0 in Eq. (12.13) is the phase of the multiply

$$\left(1 - \frac{\Omega_0^2}{\omega_0^2} - i\frac{\gamma\Omega_0}{k}\right). \tag{12.14}$$

For weak attachment ($\omega_0 < \Omega_0$), the real part of this complex number is negative. This means that for small γ the bacteria and quartz surface oscillate with the phase shift close to 180°, i.e., anti-phase. Hence, the bacterial oscillator pushes the quartz oscillator towards the equilibrium position (Fig. 12.25). This increases the restoring force and thus also increases the resonance frequency of the quartz oscillator. In the case of strong bacteria attachment ($\omega_0 > \Omega_0$), the bacterial and quartz oscillators move approximately in the same phase and the frequency decreases. Therefore, the model of coupled oscillators clearly reveals the mechanism of the apparent "negative mass" effect.

To discuss the performance and rational design of the bacterial sensor we calculated the frequency response as a function of the number of attached bacteria. Fig. 12.26 shows the results for different strengths of the elastic attachment bond. The output signal (frequency shift) is considerably stronger for strong attachment. This suggests using a strong attachment method to achieve a low bacteria detection threshold. Importantly, a substantial linear range of detection occurs that is especially broad for weak attachment. This allows finding the number of attached bacteria by calibration measurement of only the initial slope of the response curve. Additionally, we modeled the effect of inhomogeneous bacterial binding strength. Fig. 12.27 shows that for two types of binding sites with 2 and 10 MHz attachment strength, the response of a 5 MHz sensor crucially depends on the distribution of bacteria between the sites. In particular, at about 0.8/0.2 distribution, the signal is very small and thus a false negative result will be measured. This underlines the importance of using the bioreceptors with a narrow distribution of strong binding strengths.

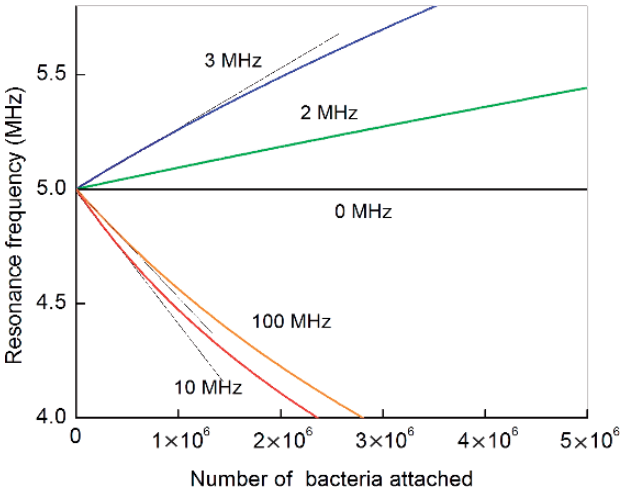

Figure 12.26. Resonance frequency as a function of the number of bacteria attached for different elastic binding strengths at 0, 2, 3, 10, and 100 MHz, as indicated. Notable is substantial linear dynamic range increasing for weaker attachment.

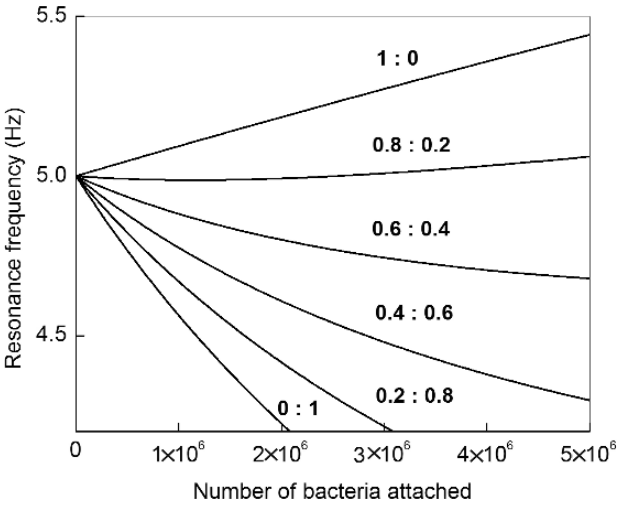

Figure 12.27. The effect of inhomogeneous bacterial binding strength on sensor. The response of a 5 MHz sensor crucially depends on distribution of bacteria between the two types of binding sites with 2 and 10 MHz attachment strength. In particular, at about 0.8/0.2 distribution, the signal is very small and thus a false negative result will be measured.

6. Conclusions

Even though acoustic wave technologies such as the TSM are not new, their adaptation to biological analysis has flourished mainly in the past decade. Most likely the next ten years will see an even larger contingent of researchers developing biosensors based on these platforms as affordability, access, sensitivity, and technical understanding increase. The most remarkable property of acoustic wave devices is their relative simplicity. The number of different devices adapted to work in the biological/medical environment is likely to expand in the future. It is therefore vital to establish a good understanding of the nature of the signals produced by acoustic wave devices when they are used for testing bacteria. The paradox of "negative mass" is a real threat to the interpretation of experimental results related to the detection of bacteria. Knowledge of the true nature of "negative mass" linked to the strength of bacteria attachment will contribute significantly to our understanding of the results of "weighing bacteria." We hope it may stimulate increased interest in the technology and motivate new experiments with a variety of microorganisms. The impact of these studies may extend beyond an appreciation of bacterial detection. One may now begin to conceive of strategies for the study and control of processes of bacterial settlement, bacterial colonization, biofilm formation, and bacterial infection in which bacterial attachment plays a role.

Acknowledgments

Our work was supported by grants from Sigma Xi Grants-in-Aid of Research (10040088), DARPA (MDA972–00–1-0011), ARO/DARPA (DAAD 19–01–10454), NIH (R21 AI055645), USDA (99–34394–7546), and Aetos Technologies Inc. We are grateful to Dr. Bryan Chin for support and dialogue, and Oleg Pustovyy for technical assistance. The views expressed in this article are those of the authors, and do not reflect the official policy or position of the United States Air Force, Department of Defense, or the U.S. Government.

References

Aberl F and Wolf H (1993) Present trends in immunosensors. LaborPraxis 70–74, 76–77

Ahluwalia A, Derossi D, Ristori C, Schirone A and Serra G (1992) A comparative study of protein immobilization techniques for optical immunosensors. Biosens. Bioelectron. 7:207–214

Ahmad A and Ahmad S (1996) Solvent effect on antibody antigen interaction. Environ. Res. 5:29–36

Aisenbrey C, Harzer U, Bauer-Manz G, Bar G, Chotimah INH, Bertani P, Sizun C, Kuhn A and Bechinger B (2006) Proton-decoupled 15N and 31P solid-state NMR investigations of the Pf3 coat protein in oriented phospholipid bilayers. FEBS Journal 273:817–828

Aizawa H, Kurosawa S, Tanaka M, Yoshimoto M, Miyake J and Tanaka H (2001) Rapid diagnosis of Treponema pallidum in serum using latex piezoelectric immunoassay. Anal. Chim. Acta 437:167–169

Alberts B, Bray D, Lewis J, Raff M, Roberts K and Watson JD (1994) Molecular biology of the cell, 3rd ed. New York: Garland Publishing

Auner GW, Shreve G, Ying H, Newaz G, Hughes C and Xu J (2003) Dual-mode acoustic wave biosensors microarrays. Proc. SPIE Int. Soc. Opt. Eng. 5119:129–139

Babacan S, Pivarnik P, Letcher S., and Rand, A.G. 2000. Evaluation of antibody immobilization methods for piezoelectric biosensor application. Biosens. Bioelectron. 15:615–621

Babacan, S., Pivarnik, P, Letcher S and Rand AG (2002) Piezoelectric flow injector analysis biosensor for the detection of Salmonella typhimurium. J. Food Sci. 61: 314–320

Bailey CA, Fiebor B, Yen W, Vodyanoy V, Cernosek RW and Chin BA (2002) Thickness shear mode (TSM) resonators used for biosensing. Proc. SPIE Int. Soc. Opt. Eng. 4575:138–149

Balasubramanian S, Sorokulova IB, Vodyanoy VJ and Simonian AL (2007) Lytic phage as a specific and selective probe for detection of Staphylococcus aureus—A surface plasmon resonance spectroscopic study. Biosens. Bioelectron. 22:948–955

Ballantine DS, White RM, Martin SJ, Ricco AJ, Zellers ET, Frye GC, Wohltjen H, Levy M and Stern R (1997) Acoustic Wave Sensors: Theory, Design, & Physico-Chemical Applications. Academic Press, San Diego

Bandey HL, Martin SJ, Cernosek RW and Hillman AR (1999) Modeling the responses of thickness-shear mode resonators under various loading conditions. Anal. Chem. 71:2205–2214

Bao L, Deng L, Nie L, Yao S and Wei W (1996a) Determination of microorganisms with a quartz crystal microbalance sensor. Anal. Chim. Acta 319:97–101

Bao L, Deng L, Nie L, Yao S and Wei W (1996b) A rapid method for determination of Proteus vulgaris with a piezoelectric quartz crystal sensor coated with a thin liquid film. Biosens. Bioelectron. 11:1193–1198

Barraud A, Perrot H, Billard V, Martelet C and Therasse J (1993) Study of immunoglobulin G thin layers obtained by the Langmuir-Blodgett method: application to immunosensors. Biosens. Bioelectron. 8:39–48

Bashtovyy D, Marsh D, Hemminga MA and Pali T (2001) Constrained modeling of spin-labeled major coat protein mutants from M13 bacteriophage in a phospholipid bilayer. Protein Sci. 10:979–987

Ben-Dov I, Willner I and Zisman E (1997) Piezoelectric immunosensors for urine specimens of Chlamydia trachomatis employing quartz crystal microbalance microgravimetric analyses. Anal. Chem. 69:3506–3512

Berg S, Johannsmann D and Ruths M (2002) Frequency response of quartz crystal shear-resonator during an adhesive, elastic contact in a surface forces apparatus. J. Appl. Phys. 92:6905–6910

Berkenpas E, Millard P and Pereira da Cunha M (2006) Detection of Escherichia coli O157:H7 with langasite pure shear horizontal surface acoustic wave sensors. Biosens. Bioelectron. 21:2255–2262

Bessueille F, Dugas V, Vikulov V, Cloarec JP, Souteyrand E and Martin JR (2005) Assessment of porous silicon substrate for well-characterized sensitive DNA chip implement. Biosens. Bioelectron. 21: 908–916

Betageri GV, Black CD, Szebeni J, Wahl LM and Weinstein JN (1993) Fc-receptor-mediated targeting of antibody-bearing liposomes containing dideoxycytidine triphosphate to human monocyte/macrophages. J. Pharm. Pharamcol. 45:48–53

Borovskya B, Krim J, Syed Asif S and Wahl K (2001) Measuring nanomechanical properties of a dynamic contact using an indenter probe and quartz crystal microbalance. J. Appl. Phys. 90:6391–6396

Branch DW and Brozik SM (2004) Low-level detection of a Bacillus anthracis simulant using love-wave biosensors on 36° YX LiTaO3. Biosens. Bioelectron. 19:849–859

Bunde RL, Jarvi EJ and Rosentreter JJ (1998) Piezoelectric quartz crystal biosensors. Talanta 46:1223–1236

Buzby JC and Roberts T (1997) Economic costs and trade impacts of microbial food-borne illness. World Health Stat. Q. 50:57–66

Bykov VA (1996) Langmuir-Blodgett films and nanotechnology. Biosens. Bioelectron. 11:923–932

Carter RM, Jacobs MB, Lubrano GJ and Guilbault GG (1995a) Piezoelectric detection of ricin and affinity-purified goat anti-ricin antibody. Anal. Lett. 28:1379–1386

Carter RM, Mekalanos JJ, Jacobs MB, Lubrano GJ and Guilbault GG (1995b) Quartz crystal microbalance detection of Vibrio cholerae O139 serotype. J. Immunol. Methods 187:121–125

Casalinuovo I, Di Pierro D, Bruno E, Di Francesco P and Coletta M (2005) Experimental use of a new surface acoustic wave sensor for the rapid identification of bacteria and yeasts. Lett. Appl. Microbiol. 42:24–29

Cavicacute BA, Hayward GL and Thompson M (1999) Acoustic waves and the study of biochemical macromolecules and cells at the sensor-liquid interface. Analyst 124:1405–1420

Chang K-S, Jang H-D, Lee C-F, Lee Y-G, Yuan C-J and Lee S-H (2006) Series quartz crystal sensor for remote bacteria population monitoring in raw milk via the Internet. Biosens. Bioelectron. 21:1581–1590

Chen M, Liu M, Yu L, Cai G, Chen Q, Wu R, Wang F, Zhang B, Jiang T and Fu W (2005) Construction of a novel peptide nucleic acid piezoelectric gene sensor microarray detection system. J. Nanosci. Nanotechnol. 5:1266–1272

Chin RC, Salazar N, Mayo MW, Villavicencio V, Taylor RB, Chambers JP and Valdes JJ (1996) Development of a bacteriophage displayed peptide library and biosensor. Proc. SPIE Int. Soc. Opt. Eng. 2680:16–26

Chothia C and Janin J (1975) Principles of protein-protein recognition. Nature 256:705–708

Chou PY and Fasman GD (1974) Prediction of protein conformation. Biochemistry 13:222–245

Clark LCJ and Lyons C (1962) Electrode systems for continuous monitoring in cardiovascular surgery. Ann. N. Y. Acad. Sci. 102:29–45

Cornell BA, Braach-Maksvytis VL, King LG, Osman PD, Raguse B, Wieczorek L and Pace RJ (1997) A biosensor that uses ion-channel switches. Nature 387:580–583

Cornell BA, Krishna G, Osman PD, Pace RD and Wieczorek L (2001) Tethered-bilayer lipid membranes as a support for membrane-active peptides. Biochem. Soc. Trans. 29:613–617

Curie J and Curie P (1880) Ann. de Chim. et Phys. 91:294

Dai J, Baker GL and Bruening ML (2006) Use of porous membranes modified with polyelectrolyte multilayers as substrates for protein arrays with low nonspecific adsorption. Anal. Chem. 78:135–140

Davies LT and Rideal EK (1963) Interfacial Phenomena. Academic Press, New York

Deisingh A and Thompson M (2001) Sequences of E. coli O157:H7 detected by a PCR-acoustic wave sensor combination. Analyst 126:2153–2158

Deng L, Tan, H, Xu Y, Nie L and Yao S (1997) On-line rapid detection of urease-producing bacteria with a novel bulk acoustic wave ammonia sensor. Enzyme Microb. Technol. 21:258–264

Deobagkar DD, Limaye V, Sinha S and Yadava RDS (2005) Acoustic wave immunosensing of Escherichia coli in water. Sens. Actuators B 104:85–89

Dickert F, Hayden O, Lieberzeit P, Palfinger C, Pickert D, Wolff U and Scholl G (2003) Borderline applications of QCM-devices: synthetic antibodies for analytes in both nm- and um-dimensions. Sens. Actuators B 95:20–24

Dickert FL, Hayden O, Bindeus R, Mann K, Blaas D and Waigmann E (2004) Bioimprinted QCM sensors for virus detection–screening of plant sap. Anal. Bioanal. Chem. 378:1929–1934

Dickert FL, Lieberzeit P and Hayden O (2003) Sensor strategies for microorganism detection–from physical principles to imprinting procedures. Anal. Bioanal. Chem. 377:540–549

Dybwad G (1985) A sensitive new method for the determination of adhesive bonding between a particle and a substrate. J. Appl. Phys. 58:2789–2790

Eun A, Huang L, Chew F, Li S and Wong S (2002) Detection of two orchid viruses using quartz crystal microbalance (QCM) immunosensors. J. Virol. Methods 99:71–79

Fan H, Lu Y, Stump A, Reed ST, Baer T, Schunk R, Perez-Luna V, Lopez GP and Brinker CJ (2000) Rapid prototyping of patterned functional nanostructures. Nature 405:56–60

World Health Organization (1997) Foodborne diseases—possibly 350 times more frequent than reported.

Frisk T, Ronnholm D, van der Wijngaart W and Stemme G (2006) A micromachined interface for airborne sample-to-liquid transfer and its application in a biosensor system. Lab. Chip 6:1504–1509

Fung YS and Wong YY (2001) Self-assembled monolayers as the coating in a quartz piezoelectric crystal immunosensor to detect Salmonella in aqueous solution. Anal. Chem. 73: 5302–5309

Furch M, Ueberfeld J, Hartmann A, Bock D and Seeger S (1996) Ultrathin oligonucleotide layers for fluorescence based DNA-sensors. Proc. SPIE Int. Soc. Opt. Eng. 2928:220–226

Gaines GLJ (1966) Insoluble Monolayers at Liquid-gas Interfaces. Interscience, New York

Gao H, Kislig E, Oranth N and Sigrist H (1994) Photolinker-polymer-mediated immobilization of monoclonal antibodies, F(ab')2 and F(ab') fragments. Biotechnol. Appl. Biochem. 20:251–263

Gao Z, Tao G and Li G (1998) Research on detection of type C2 staphylococcus enterotoxin in food with piezoelectric immunosensors. Wei Sheng Yan Jiu 27:122–124

Garnier J, Osguthorpe DJ and Robson B (1978) Analysis of the accuracy and implications of simple methods for predicting the secondary structure of globular proteins. J. Mol. Biol. 120:97–120

Gawrisch K, Gaede HC, Luckett KM, Polozov IV and Yeliseev A (2005) Solid-supported membranes inside porous substrates and their use in biosensors, WIPO Patent WO/2005/069004 http://www.wipo.int/pctdb/en/ia.jsp?IA=US2005/ 000069&LANGUAGE=EN (accessed April 11, 2007)

Ghafouri S and Thompson M (1999) Interfacial properties of biotin conjugate avidin complexes studied by acoustic wave sensor. Langmuir 15:564–572

Gizeli E (2002) Biomolecular Sensors. Taylor & Francis, Inc., New York, pp 176–206

Goldman ER, Pazirandeh MP, Charles PT, Balighian E.D and Anderson GP (2002) Selection of phage displayed peptides for the detection of 2,4,6-trinitrotoluene in seawater. Anal. Chim. Acta 457:13–19

Goldman ER, Pazirandeh MP, Mauro JM, King KD, Frey JC and Anderson GP (2000) Phage-displayed peptides as biosensor reagents. J. Mol. Recognit. 13:382–387

Goodchild S, Love T, Hopkins N and Mayers C (2006) Engineering antibodies for biosensor technologies. Adv. Appl. Microbiol. 58:185–226

Grate JW and Frye GC (1996) Acoustic wave sensors. Sens. Update 2:37–83

Griffith J, Manning M and Dunn K (1981) Filamentous bacteriophage contract into hollow spherical particles upon exposure to a chloroform-water interface. Cell 23:747–753

Harteveld JLN, Nieuwenhuizen MS and Wils ERJ (1997) Detection of staphylococcal enterotoxin B employing a piezoelectric crystal immunosensor. Biosens. Bioelectron. 12:661–667

Hayden O, Bindeus R and Dickert FL (2003) Combining atomic force microscope and quartz crystal microbalance studies for cell detection. Meas. Sci. Technol. 14: 1876–1881

Hayden O and Dickert FL (2001) Selective microorganism detection with cell surface imprinted polymers. Adv. Mater. 13:1480–1483

He F, Geng Q, Zhu W, Nie L, Yao S and Meifeng C (1994) Rapid detection of Escherichia coli using a separated electrode piezoelectric crystal sensor. Anal. Chim. Acta 289:313–319

He F and Zhang L (2002) Rapid diagnosis of M. tuberculosis using a piezoelectric immunosensor. Anal. Sci. 18:397–401

He F, Zhang X, Zhou J and Liu Z (2006) A new MSPQC system for rapid detection of pathogens in clinical samples. J. Microbiol. Methods 66:56–62

He F, Zhao J, Zhang L and Su X (2003) A rapid method for determining Mycobacterium tuberculosis based on a bulk acoustic wave impedance biosensor. Talanta 59:935–941

He F and Zhou J (2007) A new antimicrobial susceptibility testing method of Escherichia coli against ampicillin by MSPQC. J. Microbiol. Methods 68:563–567

Herriott RM and Barlow JL (1957) The protein coats or "ghosts" of Escherichia coli phage T2. Preparation, assay, and some chemical properties. J. Gen. Physiol. 40:809–825

Horisberger M (1984) Electron-opaque markers: a review. In: Polak JM and Varndell IM (eds) Immunolabelling for Electron Microscopy. Elsevier, Amsterdam

Horisberger M (1992) Colloidal gold and its application in cell biology. Int. Rev. Cytol. 136:227–87

Houbiers MC and Hemminga MA (2004) Protein-lipid interactions of bacteriophage M13 gene 9 minor coat protein. Mol. Membr. Biol. 21:351–359

Houbiers MC, Wolfs CJAM, Spruijt RB, Bollen YJM, Hemminga MA and Goormaghtigh E (2001) Conformation and orientation of the gene 9 minor coat protein of bacteriophage M13 in phospholipid bilayers. Biochim. Biophys. Acta Biomembr. 1511:224–235

Howe E and Harding G (2000) A comparison of protocols for the optimisation of detection of bacteria using a surface acoustic wave (SAW) biosensor. Biosens. Bioelectron. 15:641–649

Im W and Brooks CL (2004) De novo folding of membrane proteins: an exploration of the structure and NMR properties of the fd coat protein. J. Mol. Biol. 337:513–519

Ishimori Y, Karube I and Suzuki IS (1981) Determination of microbial populations with piezoelectric membranes. Appl. Environ. Microbiol. 42:632–637

Ivnitski D, Abdel-Hamid I, Atanasov P and Wilkins E (1999) Biosensors for detection of pathogenic bacteria. Biosens. Bioelectron. 14:599–624

Janshoff A, Galla HJ and Steinem C (2000) Piezoelectric mass-sensing devices as biosensors-an alternative to optical biosensors? Angew. Chem. Int. Ed. Engl. 39:4004–4032

Janshoff A and Steinem C (2001) Quartz crystal microbalance for bioanalytical applications. Sens. Update 9:313–354

Janshoff A, Steinem C and Wegener J (2004) Noninvasive Electrical Sensor Devices to Monitor Living Cells Online. Ultrathin Electrochemical Chemo- and Biosensors. Springer, New York

Jiang Y-B, Liu N, Gerung H, Cecchi JL and Brinker CJ (2006) Nanometer-thick conformal pore sealing of self-assembled mesoporous silica by plasma-assisted atomic layer deposition. J. Am. Chem. Soc. 128:11018–11019

Kaspar M, Stadler H, Weiss T and Ziegler C (2000) Thickness shear mode resonators ("mass sensitive devices") in bioanalysis. Fresenius J. Anal. Chem. 366:602–610

Kim G-H, Rand AG and Letcher SV (2003) Impedance characterization of a piezoelectric immunosensor part II: Salmonella typhimurium detection using magnetic enhancement. Biosens. Bioelectron. 18:91–99

Kim N and Park I-S (2003) Application of a flow-type antibody sensor to the detection of Escherichia coli in various foods. Biosens. Bioelectron. 18:1101–1107

Kim N, Park I-S and Kim D-K (2004) Characteristics of a label-free piezoelectric immunosensor detecting Pseudomonas aeruginosa. Sens. Actuators B 100:432–438

King WH (1964) Piezoelectric sorption detector. Anal. Chem. 36:1735–1739

Kleinschmidt AK, Lang D, Jacherts D and Zahn RK (1962) Preparation and length measurements of the total deoxyribonucleic acid (DNA) content of T2 bacteriophages. Biochim. Biophys. Acta 61:875–864

Konig B and Gratzel M (1993) Detection of viruses and bacteria with piezoelectric immunosensors. Anal. Lett. 26:1567–1585

Konig B and Gratzel M (1995) A piezoelectric immunosensor for hepatitis viruses. Anal. Chim. Acta 309:19–25
Kouzmitcheva G (2005) Personal communication.
Krause R (1993) Process control for Ni/Au plating with QCM technology. Circuitree 6:10–12
Kreth J, Hagerman E, Tam K, Merritt J, Wong D, Wu B, Myung N, Shi W and Qi F (2004) Quantitative analyses of Streptococcus mutans biofilms with quartz crystal microbalance, microjet impingement and confocal microscopy. Biofilms 1:277–284
Kurosawa S, Park J, Aizawa H, Wakida S, Tao H and Ishihara K (2006) Quartz crystal microbalance immunosensors for environmental monitoring. Biosens. Bioelectron. 22:473–481
Lakshmanan RS, Hu J, Guntupalli R, Wan J, Huang S, Yang H, Petrenko VA, Barbaree JM and Chin BA (2006) Detection of Salmonella typhimurium using phage based magnetostrictive sensor. Proc. SPIE Int. Soc. Opt. Eng. 6218:62180Z
Lazcka O, Campo FJD and Munoz FX (2007) Pathogen detection: A perspective of traditional methods and biosensors. Biosens. Bioelectron. 22:1205–1217
Le D, He F-J, Jiang TJ, Nie L and Yao S (1995) A goat-anti-human IgG modified piezoimmunosensor for Staphylococcus aureus detection. J. Microbiol. Methods 23:229–234
Leonard P, Hearty S, Brennan J, Dunne L, Quinn J, Chakraborty T and O'Kennedy R (2003) Advances in biosensors for detection of pathogens in food and water. Enzyme Microb. Technol. 32:3–13
Lin H-C and Tsai W-C (2003) Piezoelectric crystal immunosensor for the detection of staphylococcal enterotoxin B. Biosens. Bioelectron. 18:1479–1483
Love AEH (1911) Some problems of geodynamics. Cambridge: Cambridge
Lucklum R (2005) Non-gravimetric contributions to QCR sensor response. Analyst 130:1465–1473
Mao X, Yang L, Su X-L and Li Y (2006) A nanoparticle amplification based quartz crystal microbalance DNA sensor for detection of Escherichia coli O157:H7. Biosens. Bioelectron. 21:1178–1185
Martin SJ, Granstaff VE and Frye GC (1991) Characterization of quartz crystal microbalance with simultaneous mass and liquid loading. Anal. Chem. 63:2272–2281
Marxer C, Coen M, Greber T, Greber U and Schlapbach L (2003) Cell spreading on quartz crystal microbalance elicits positive frequency shifts indicative of viscosity changes. Anal. Bioanal. Chem. 377:578–586
Mead P, Slutsker L, Dietz V, McCaig L, Bresee J, Shapiro C, Griffin P and Tauxe RV (1999) Food-related illness and death in the United States. Emerg. Infect. Dis. 5:607–625
Minunni M, Skladal P and Mascini M (1994) A piezoelectric quartz crystal biosensor as a direct affinity sensor. Anal. Lett. 27:1475–1487
Mittler-Neher S, Spinke J, Liley M, Nelles G, Weisser M, Back R, Wenz G and Knoll W (1995) Spectroscopic and surface-analytical characterization of self-assembled layers on Au. Biosens. Bioelectron. 10:903–916
Mo X-T, Zhou Y-P, Lei H and Deng L (2002) Microbalance-DNA probe method for the detection of specific bacteria in water. Enzyme Microb. Technol. 30:583–589
Moll N, Pascal E, Dinh DH, Pillot J-P, Bennetau B, Rebiere D, Moynet D, Mas Y, Mossalayi D, Pistre J and Dejous C (2007) A Love wave immunosensor for whole E. coli bacteria detection using an innovative two-step immobilisation approach. Biosens. Bioelectron. 22:2145–2150
Morgan DP (2000) A history of surface acoustic wave devices. Int. J. High Speed Electron. Syst. 10:553–602
Muramatsu H, Kajiwara K, Tamiya E, Karube I (1986) Piezoelectric immunosensor for the detection of Candida albicans microbes. Anal. Chim. Acta 188:257–261
Muratsugu M, Ohta F, Miya Y, Hosokawa T, Kurosawa S, Kamo N and Ikeda H (1993) Quartz crystal microbalance for the detection of microgram quantities of human serum albumin: relationship between the frequency change and the mass of protein adsorbed. Anal. Chem. 65:2933–2937
Nakanishi K, Karube I, Hiroshi S, Uchida A and Ishida Y (1996) Detection of the red tide-causing plankton Chattonella marina using a piezoelectric immunosensor. Anal. Chim. Acta 325:73–80
Nanduri V (2005) Phage at the air-liquid interface for the fabrication of biosensors. Doctoral Dissertation. graduate.auburn.edu/auetd Auburn University, Alabama
Nanduri V, Sorokulova IB, Samoylov AM, Simonian AL, Petrenko VA, Vodyanoy V (2007) Phage as a molecular recognition element in biosensors immobilized by physical adsorption. Biosens. Bioelectron. 22:986–992
Neidhardt FC (1987) Escherichia coli and Salmonella. American Society For Microbiology, Washington, D.C.
Nishiyama Y, Tanaka S, Hillhouse HW, Nishiyama N, Egashira Y and Ueyama K (2006) Synthesis of ordered mesoporous zirconium phosphate films by spin coating and vapor treatments. Langmuir 22:9469–9472
Niven D, Chambers J, Anderson T and White D (1993) Long-term, on-line monitoring of microbial biofilms using a quartz crystal microbalance. Anal. Chem. 65:65–69
O'Sullivan CK and Guilbault GG (1999) Commercial quartz crystal microbalances—theory and applications. Biosens. Bioelectron. 14:663–670
Olsen EV (2000) Functional durability of a quartz crystal microbalance sensor for the rapid detection of Salmonella in liquids from poultry packaging. Masters Thesis. http://graduate.auburn.edu/auetd Auburn University, Alabama (accessed April 10, 2007)

Olsen EV (2005) Phage-coupled piezoelectric biodetector for Salmonella typhimurium. Doctoral Dissertation. http://graduate.auburn.edu/auetd Auburn University, Alabama (accessed April 10, 2007)

Olsen EV, Pathirana ST, Samoylov AM, Barbaree JM, Chin BA, Neely WC and Vodyanoy V (2003) Specific and selective biosensor for Salmonella and its detection in the environment. J. Microbiol. Methods 53:273–285

Olsen EV, Sorokulova IB, Petrenko VA, Chen IH, Barbaree JM and Vodyanoy VJ (2006) Affinity-selected filamentous bacteriophage as a probe for acoustic wave biodetectors of Salmonella typhimurium. Biosens. Bioelectron. 21:1434–1442

Olsen EV, Sykora JC, Sorokulova IB, Chen I-H, Neely WC, Barbaree JM, Petrenko VA and Vodyanoy VJ (2007) Phage fusion proteins as bioselective receptors for piezoelectric sensors. Electrochem. Soc. Trans. 2:9–25

Otto K, Elwing H and Hermansson M (1999) Effect of ionic strength on initial interactions of Escherichia coli with surfaces, studied on-line by a novel quartz crystal microbalance technique. J. Bacteriol. 181:5210–5218

Ozen A, Montgomery K, Jegier P, Patterson S, Daumer KA, Ripp SA, Garland JL and Sayler GS (2004) Development of bacteriophage-based bioluminescent bioreporters for monitoring of microbial pathogens. Proc. SPIE Int. Soc. Opt. Eng. 5270:58–68

Park I-S and Kim N (1998) Thiolated Salmonella antibody immobilization onto the gold surface of piezoelectric quartz crystal. Biosens. Bioelectron. 13:1091–1097

Park I-S, Kim W-Y and Kim N (2000) Operational characteristics of an antibody-immobilized QCM system detecting Salmonella spp. Biosens. Bioelectron. 15:167–172

Pathirana S, Myers LJ, Vodyanoy V and Neely WC (1996) Assembly of cadmium stearate and valinomycin molecules assists complexing of K+ in mixed Langmuir-Blodgett films. Supramol. Sci. 2:149–154

Pathirana S, Neely WC, Myers LJ and Vodyanoy V (1992) Interaction of valinomycin and stearic acid in monolayers. Langmuir 8:1984–1987

Pathirana S, Neely WC and Vodyanoy V (1998) Condensing and expanding the effects of the odorants (+)- and (−)-carvone on phospholipid monolayers. Langmuir 14:679–682

Pathirana ST (1993) Interaction of valinomycin and stearic acid in monolayers at the air/water interface. Doctoral Dissertation. Auburn University, Alabama

Pathirana ST, Barbaree J, Chin BA, Hartell MG, Neely WC and Vodyanoy V (2000) Rapid and sensitive biosensor for Salmonella. Biosens. Bioelectron. 15:135–141

Pattus F, Desnuelle P and Verger R (1978) Spreading of liposomes at the air/water interface. Biochim. Biophys. Acta 507:62–70

Pattus F and Rothen C (1981) Lipid-protein interactions in monolayers at the air-water interface. In: Azzi A, Brodbeck U, Zahler P (eds) Membrane Proteins. Springer-Verlag, Berlin pp 229–240

Pattus F, Rothen C, Streit M and Zahler P (1981) Further studies on the spreading of biomembranes at the air/water interface. Structure, composition, enzymatic activities of human erythrocyte and sarcoplasmic reticulum membrane films. Biochim. Biophys. Acta Biomembr. 647:29–39

Pavey KD (2002) Quartz crystal analytical sensors: the future of label-free, real-time diagnostics? Expert Rev. Mol. Diag. 2:173–186

Pavey KD, Ali Z, Olliff CJ and Paul F 1999. Application of the quartz crystal microbalance to the monitoring of Staphylococcus epidermidis antigen-antibody agglutination. J. Pharm. Biomed. Anal. 20:241–245

Pavey KD, Barnes L, Hanlon G, Olliff C, Ali Z and Paul F (2001) A rapid, non-destructive method for the determination of Staphylococcus epidermidis adhesion to surfaces using quartz crystal resonant sensor technology. Lett. Appl. Microbiol. 33:344–348

Pereira de Jesus D, Naves C and Lucia do Lago C (2002) Determination of boron by using a quartz crystal resonator coated with N-Methyl-D-glucamine-modified poly(epichlorohydrin). Anal. Chem. 74:3274–3280

Petrenko VA (2004) Personal communication.

Petrenko VA and Smith GP (2000) Phages from landscape libraries as substitute antibodies. Protein Eng. 13:589–592

Petrenko VA, Sorokulova IB, Chin BA, Barbaree JM, Vodyanoy VJ, Chen IH and Samoylov AM (2005) Biospecific peptide probes against Salmonella isolated from phage display libraries, and their diagnostic and drug delivery uses. US Patent Application 20050137136, filed Apr 29, 2004

Petrenko VA and Vodyanoy VJ (2003) Phage display for detection of biological threat agents. J. Microbiol. Methods 53:253–262

Petrenko VA, Vodyanoy VJ and Sykora JC (2007) Methods of forming monolayers of phage-derived products and uses thereof. US Patent #7, 267, 993

Petty MC (1991) Application of multilayer films to molecular sensors: some examples of bioengineering at the molecular level. J. Biomed. Eng. 13:209–214

PM-740 Series Operation and Service Manual. (1996) Maxtek, Inc., Sante Fe Springs, California

Pohanka M and Skládal P (2005) Piezoelectric immunosensor for Francisella tularensis detection using immunoglobulin M in a limiting dilution. Anal. Lett. 38:411–422

Prusak-Sochaczewski E and Luong JHT (1990) Development of a piezoelectric immunosensor for the detection of Salmonella typhimurium. Enzyme and Microb. Technol. 12:173–177

Pyun JC, Beutel H, Meyer JU and Ruf HH (1998) Development of a biosensor for E. coli based on a flexural plate wave (FPW) transducer. Biosens. Bioelectron 13:839–845

Qu X, Bao L, Su X and Wei W (1998) Rapid detection of Escherichia coliform with a bulk acoustic wave sensor based on the gelation of Tachypleus amebocyte lysate. Talanta 47:285–290

Ramirez E, Mas JM, Carbonell X, Aviles FX and Villaverde A (1999) Detection of molecular interactions by using a new peptide-displaying bacteriophage. Biosensor. Biochem. Biophys. Res. Commun. 262:801–805

Ramsden JJ (1997a) Dynamics of protein adsorption at the solid/liquid interface. Recent Res. Dev. Phys. Chem. 1:133–142

Ramsden JJ (1997b) Protein adsorption at the solid/liquid interface. Conference on Colloid Chemistry: In Memoriam Aladar Buzagh, Proceedings, 7th, Eger, Hung., Sept. 23–26, 1996, 148–151

Ramsden JJ (1998) Biomimetic protein immobilization using lipid bilayers. Biosens. Bioelectronics 13:593–598

Ramsden JJ (1999) On protein-lipid membrane interactions. Colloids Surfaces B Biointerfaces 14:77–81

Ramsden JJ (2001) Multiple interactions in protein-membrane binding. NATO Science Series, 335:244–269. IOS Press, Amsterdam

Rayleigh L (1885) On waves propagating along the plane surface of an elastic solid. Proc. London Math. Soc. 17:4–11

Reipa V, Almeida J and Cole KD (2006) Long-term monitoring of biofilm growth and disinfection using a quartz crystal microbalance and reflectance measurements. J. Microbiol. Methods 66:449–459

Rickert J, Gopel W, Hayward GL, Cavic BA and Thompson M (1999) Biosensors based on acoustic wave devices. Sens. Update 5:105–139

Roberts LM and Dunker AK (1993) Structural changes accompanying chloroform-induced contraction of the filamentous phage fd. Biochemistry 32:10479–10488

Samoylov AM, Samoylova TI, Hartell MG, Pathirana ST, Smith BF and Vodyanoy V (2002a) Recognition of cell-specific binding of phage display derived peptides using an acoustic wave sensor. Biomol. Eng. 18:269–272

Samoylov AM, Samoylova TI, Pathirana ST, Globa LP and Vodyanoy VJ (2002b) Peptide biosensor for recognition of cross-species cell surface markers. J. Mol. Recognit. 15:197–203

Sauerbrey GZZ (1959) Use of quartz vibrator for weighing thin films on a microbalance. Z. Phys. 155:206–212

Sayler GS, Ripp SA, Applegate BM (2003) Bioluminescent biosensor device. US Patent Application 20030027241, filed July 20, 2001

Scherz P (2000) Oscillators and Timers. McGraw-Hill, Inc., New York

Selz KA, Samoylova TI, Samoylov AM, Vodyanoy VJ and Mandell AJ (2006) Designing allosteric peptide ligands targeting a globular protein. Biopolymers 85:38–59

Si S, Lia X, Fungb Y and Zhub D (2001) Rapid detection of Salmonella enteritidis by piezoelectric immunosensor. Microchem. J. 68:21–27

Si S, Ren F, Cheng W and Yao S (1997) Preparation of a piezoelectric immunosensor for the detection of Salmonella paratyphi A by immobilization of antibodies on electropolymerized films. Fresenius J. Anal. Chem. 357:1101–1105

Skládal P (2003) Piezoelectric quartz crystal sensors applied for bioanalytical assays and characterization of affinity interactions. J. Braz. Chem. Soc. 14:491–502

Sobotka H and Trurnit HJ (1961) Need title of their article here. In: Alexander P, Block RJ (eds) Analytical Methods of Protein Chemistry. Pergamon Press, Oxford, UK, pp 212–243

Song M-J, Yun D-H, Jin J-H, Min N-K and Hong S-I (2006) Comparison of effective working electrode areas on planar and porous silicon substrates for cholesterol biosensor. Jpn. J. Appl. Phys. 45:7197–7202

Sorial J and Lec R (2004) A piezoelectric interfacial phenomena biosensor. Masters Thesis. http://dspace.library.drexel.edu/handle/1860/82 Drexel University, Pennsylvania (accessed April 10, 2007)

Sorokulova IB, Olsen EV, Chen IH, Fiebor B, Barbaree JM, Vodyanoy VJ, Chin BA and Petrenko VA (2005) Landscape phage probes for Salmonella typhimurium. J. Microbiol. Methods 63:55–72

Spangler BD, Wilkinson EA, Murphy JT and Tyler BJ (2001) Comparison of the Spreeta®surface plasmon resonance sensor and a quartz crystal microbalance for detection of Escherichia coli heat-labile enterotoxin. Anal. Chim. Acta 444:149–161

Stadler H, Mondon M and Ziegler C (2003) Protein adsorption on surfaces: dynamic contact angle (DCA) and quartz-crystal microbalance (QCM) measurements. Anal. Bioanal. Chem 375:53–61

Storri S, Santoni T and Mascini M (1998) A piezoelectric biosensor for DNA hybridisation detection. Anal. Lett. 31:1795–1808

Su C-C, Wu T-Z, Chen L-K, Yang H-H and Tai D-F (2003) Development of immunochips for the detection of dengue viral antigens. Anal. Chim. Acta 479:117–123

Su X-L and Li SFY (2001) Serological determination of Helicobacter pylori infection using sandwiched and enzymatically amplified piezoelectric biosensor. Anal. Chim. Acta 429:27–36

Su X-L and Li Y (2004) A self-assembled monolayer-based piezoelectric immunosensor for rapid detection of Escherichia coli O157:H7. Biosens. Bioelectron. 19:563–574

Su X-L and Li Y (2005) A QCM immunosensor for Salmonella detection with simultaneous measurements of resonant frequency and motional resistance. Biosens. Bioelectron. 21:840–848

Su X, Low S, Kwang J, Chew VHT and Li SFY (2001) Piezoelectric quartz crystal based veterinary diagnosis for Salmonella enteritidis infection in chicken and egg. Sens. Actuators B 75:29–35

Sukhorukov GB, Montrel MM, Petrov AI, Shabarchina LI and Sukhorukov BI (1996) Multilayer films containing immobilized nucleic acids. Their structure and possibilities in biosensor applications. Biosens. Bioelectron. 11:913–922

Sykora JC (2003) Monolayers of biomolecules for recognition and transduction in biosensors. Doctoral Dissertation. Auburn University, Al. http://graduate.auburn.edu/auetd (accessed April 10, 2007)

Sykora JC, Neely WC and Vodyanoy V (2004) Solvent effects on amphotericin B monolayers. J. Colloid Interface Sci. 269:499–502

Tabacco MB, Qian X and Russo J (2004) Fluorescent virus probes for identification of bacteria. US Patent Application 20040191859, filed Mar 24, 2003

Tai D, Lin C, Wu T, Huang J and Shu P (2006) Artificial receptors in serologic tests for the early diagnosis of dengue virus infection. Clin. Chem. 58:1486–1491

Tan H, Deng L, Nie L and Yao S (1997) Detection and analysis of the growth characteristics of Proteus vulgaris with a bulk acoustic wave ammonia sensor. Analyst 122:179–184

Thompson M, Arthur C and Dhaliwal G (1986) Liquid-phase piezoelectric and acoustic transmission studies of interfacial immunochemistry. Anal. Chem. 58:1206–1209

Thompson M, Kiplingt A, Duncan-Hewitt W, Rajakovic L and Cavic-Vlasak B (1991) Thickness-shear-mode acoustic wave sensors in the liquid phase: a review. Analyst 116:881–890

Thust M, Schoning MJ, Schroth P, Malkoc U, Dicker CI, Steffen A, Kordos P and Luth H (1999) Enzyme immobilization on planar and porous silicon substrates for biosensor applications. J. Mol. Catal. B: Enzym. 7:77–83

Tiefenauer LX, Kossek S, Padeste C and Thiebaud P (1997) Towards amperometric immunosensor devices. Biosens. Bioelectron. 12:213–223

Trurnit HJ (1960) The spreading of protein monolayers. J. Colloid Sci. 15:1–13

Umezawa Y (1996) CRC handbook of ion-selective electrodes: selectivity coefficients. CRC Press, Boca Raton, Florida

Uttenthaler E, Kolinger C and Drost S (1998) Quartz crystal biosensor for detection of the African Swine Fever disease. Anal. Chim. Acta 362:91–100

Uttenthaler E, Schraml M, Mandel J and Drost S (2001) Ultrasensitive quartz crystal microbalance sensors for detection of M13-Phages in liquids. Biosens. Bioelectronics 16:735–743

Uzawa H, Kamiya S, Minoura N, Dohi H, Nishida Y, Taguchi K, Yokoyama S, Mori H, Shimizu T and Kobayashi K (2002) A quartz crystal microbalance method for rapid detection and differentiation of shiga toxins by applying a monoalkyl globobioside as the toxin ligand. Biomacromolecules 3:411–414

Vaughan RD, O'Sullivan CK and Guilbault GG (2001) Development of a quartz crystal microbalance (QCM) immunosensor for the detection of Listeria monocytogenes. Enzyme Microb. Technol. 29:635–638

Vaughan TJ, Williams AJ, Pritchard K, Osbourn JK, Pope AR, Earnshaw JC, McCafferty J, Hodits RA, Wilton J and Johnson KS (1996) Human antibodies with sub-nanomolar affinities isolated from a large non-immunized phage display library. Nature Biotechnol. 14:309–314

Victorov IA (1967) Rayleigh and Lamb Waves—physical theory and applications. Plenum Press, New York

Vig J and Ballato A (1998) Comments about the effects of non-uniform mass loading on a quartz crystal microbalance. IEEE Trans. Ultrason. Ferroelectrics Freq. Contr. 45:1123–1124

Vodyanoy V (1994) Functional reconstitution of mammalian olfactory receptor. Report. ARO-27364.10-LS

Voinova MV, Jonson M and Kasemo B (2002) "Missing mass" effect in biosensor's QCM applications. Biosens. Bioelectron. 17:835–841

Volker M and Siegmund HU (1997) Forster energy transfer in ultrathin polymer layers as a basis for biosensors. EXS 80:175–191

Wang J, Fu W, Liu M, Wang Y, Xue Q, Huang J and Zhu Q (2002) Multichannel piezoelectric genesensor for the detection of human papilloma virus. Chinese Med. J. (Engl) 115:439–442

White RM and Voltmer FW (1965) Direct piezoelectric coupling to surface elastic waves. Appl. Phys. Lett. 7:314–316

Wong YY, Ng SP, Ng MH, Si SH, Yao SZ and Fung YS (2002) Immunosensor for the differentiation and detection of Salmonella species based on a quartz crystal microbalance. Biosens. Bioelectron. 17:676–684

Wu T-Z, Su C-C, Chen L-K, Yang H-H, Tai D-F and Peng K-C (2005) Piezoelectric immunochip for the detection of dengue fever in viremia phase. Biosens. Bioelectron. 21:689–695

Wu Z-Y, Shen G-L, Li Z-Q, Wang S-P and Yu R-Q (1999) A direct immunoassay for Schistosoma japonium antibody (SjAb) in serum by piezoelectric body acoustic wave sensor. Anal. Chim. Acta 398:57–63

Wu Z, Wu J, Wang S, Shen G and Yu R (2006) An amplified mass piezoelectric immunosensor for Schistosoma japonicum. Biosens. Bioelectron. 22:207–212

Xomeritakis G, Liu NG, Chen Z, Jiang YB, Koehn R, Johnson PE, Tsai CY, Shah PB, Khalil S, Singh S and Brinker CJ (2007) Anodic alumina supported dual-layer microporous silica membranes. J. Membr. Sci. 287:157–161

Yakhno T, Sanin A, Pelyushenko A, Kazakov V, Shaposhnikova O, Chernov A, Yakhno V, Vacca C, Falcione F and Johnson B (2007) Uncoated quartz resonator as a universal biosensor. Biosens. Bioelectron. 22:2127–2131

Yao S, Tan H, Zhang H, Su X and Wei W (1998) Bulk acoustic wave bacterial growth sensor applied to analysis of antimicrobial properties of tea. Biotechnol. Prog. 14:639–644

Ye J, Letcher S and Rand AG (1997) Piezoelectric biosensor for the detection of Salmonella typhimurium. J. Food Sci. 62:1067–1071, 1086

Yilma S, Cannon-Sykora J, Samoylov A, Lo T, Liu N, Brinker CJ, Neely WC and Vodyanoy V (2007a) Large-conductance cholesterol-amphotericin B channels in reconstituted lipid bilayers. Biosens. Bioelectron. 22:1359–1367

Yilma S, Liu N, Samoylov A, Lo T, Brinker CJ and Vodyanoy V (2007b) Amphotericin B channels in phospholipid membrane-coated nanoporous silicon surfaces: implications for photovoltaic driving of ions across membranes. Biosens. Bioelectron. 22:1605–1611

Ying-Sing F, Shi-Hui S and De-Rong Z (2000) Piezoelectric crystal for sensing bacteria by immobilizing antibodies on divinylsulphone activated poly-m-aminophenol film. Talanta 51:151–158

Yun D-H, Song M-J, Hong S-I, Kang M-S and Min N-K (2005) Highly sensitive and renewable amperometric urea sensor based on self-assembled monolayer using porous silicon substrate. J. Kor. Phys. Soc. 47:S445–S449

Zhang J, Xie Y, Dai X, Wei W (2001) Monitoring of Lactobacillus fermentation process by using ion chromatography with a series piezoelectric quartz crystal detector. J. Microbiol. Methods 44:105–111

Zhang S, Wei W, Zhang J, Mao Y and Liu S (2002) Effect of static magnetic field on growth of Escherichia coli and relative response model of series piezoelectric quartz crystal. Analyst 127:373–377

Zhao J, Zhu W and He F (2005) Rapidly determining E. coli and P. aeruginosa by an eight channels bulk acoustic wave impedance physical biosensor. Sens. Actuators B 107: 271–276

Zhou X, Liu L, Hu M, Wang L and Hu J (2002) Detection of hepatitis B virus by piezoelectric biosensor. J. Pharmaceut. Biomed. Anal. 27:341–345

Zuo B, Li S, Guo Z, Zhang J and Chen C (2004) Piezoelectric immunosensor for SARS-associated coronavirus in sputum. Anal. Chem. 76:3536–3540